Materials Today Chemistry 49 (2025) 103059

Contents lists available at ScienceDirect

Materials Today Chemistry

journal homepage: www.journals.elsevier.com/materials-today-chemistry/

PVA/casein/chitosan-based hydrogels with antioxidant bioactive agents for diabetic wound treatment

M. Gonçalves [a], A.C. Branco [a,b], V. Silva [c], D.C. Silva [a,b], M. Salema-Oom [b], J. Coelho [a], R. Colaço [d], R. Galante [e,*], P. Poeta [c], B. Saramago [a], A.P. Serro [a,b,**]

[a] Centro de Química Estrutural (CQE), Chemical Engineering Department, Institute of Molecular Sciences, Instituto Superior Técnico, University of Lisbon, Lisbon, Portugal
[b] Egas Moniz Centre for Interdisciplinary Research (CiiEM), Egas Moniz School of Health & Science, Caparica, Portugal
[c] Microbiology and Antibiotic Resistance Team (MicroART), Department of Veterinary Sciences, University of Trás-os-Montes e Alto Douro, Vila Real, Portugal
[d] Instituto de Engenharia Mecânica (IDMEC), Mechanical Engineering Department, Instituto Superior Técnico, University of Lisbon, Lisbon, Portugal
[e] Centro de Inovação em Materiais e Produtos Avançados, (CIMPA), Azores, Portugal

ARTICLE INFO

Keywords:
Hydrogel
Wound dressing
Antioxidant
Antimicrobial
Casein
Chitosan
Polyvinyl alcohol (PVA)

ABSTRACT

Wound healing is a complex process, especially in chronic conditions such as diabetes mellitus, often hindered by a prolonged inflammatory stage. Modern wound dressings aim to protect wound beds and accelerate the healing process. Hydrogel dressings have raised special interest due to their ability to retain moisture. This work focused on developing innovative wound dressings with antioxidant properties to improve the healing of chronic wounds, namely through the regulation of the oxidative environment in diabetic wounds. A base hydrogel composed of polyvinyl alcohol (PVA)/casein/chitosan was produced by freeze-thawing method. Astaxanthin and ozonized oils were incorporated in the formulation in different amounts. In general, all hydrogels presented adequate physical, chemical and biological properties to be used as dressing materials, but the ozonized oil containing hydrogel BOz12_2 stood out as the most promising one. Its porous and hydrophilic network provided high water retention and an adequate water vapor transmission rate, while maintaining structural integrity with a slow degradation profile and suitable mechanical strength. The material also exhibited moderate mucoadhesion, ensuring sufficient adherence without compromising wound removal. Importantly, it proved to be non-toxic, non-irritant, and hemocompatible, while simultaneously showing strong antioxidant activity and selective antimicrobial efficacy, including inhibition of vancomycin-resistant *Enterococcus faecium* strains.

1. Introduction

Diabetes mellitus is a chronic metabolic disorder characterized by impaired regulation of blood glucose due to insufficient insulin production or cellular resistance [1]. It affects over 500 million adults worldwide and is associated with severe complications, including impaired wound healing [2]. Chronic diabetic wounds, such as foot ulcers, are particularly problematic due to persistent inflammation, high risk of infection, and delayed tissue regeneration, often resulting in amputation. These wounds present a major burden to healthcare systems and remain a clinical and technological challenge [3–5].

Managing diabetic wounds is complicated by their underlying pathophysiology, which involves permanent inflammation, improper neovascularization, and overproduction of reactive oxygen species (ROS) [6,7]. Although ROS are needed to promote the wound healing, an excess of ROS sustains and deregulates inflammation, which impairs the healing process [8]. Maintaining an adequately moist environment is particularly critical, as desiccation impairs granulation and epithelialization. Advanced wound dressings can actively support healing by not only protecting the wound but also modulating the microenvironment to favour regeneration, especially in cases where traditional treatments are insufficient.

Hydrogels have emerged as promising materials for treating diabetic wounds. These materials are three-dimensional networks of hydrophilic polymers capable of retaining a substantial amount of water (70–90 %), which helps to maintain a moist environment [9]. The selection of

* Corresponding author.
** Corresponding author. Centro de Química Estrutural (CQE), Instituto Superior Técnico, Av. Rovisco Pais 1, 1049-001 Lisbon, Portugal.
E-mail addresses: raquelgalante@cimpa.pt (R. Galante), anapaula.serro@tecnico.ulisboa.pt (A.P. Serro).

https://doi.org/10.1016/j.mtchem.2025.103059
Received 8 July 2025; Received in revised form 14 September 2025; Accepted 17 September 2025
Available online 23 September 2025

hydrogel polymers is crucial for addressing specific therapeutic needs. Furthermore, hydrogels can be engineered to directly deliver therapeutic agents able to tackle specific problems of diabetic wounds, such as excessive inflammation and impaired vascularization.

Polyvinyl alcohol (PVA) and chitosan (Fig. 1A and B) are well-established polymers in wound healing applications due to their biocompatibility, tunable mechanical properties, and inherent antimicrobial activity [10–15]. PVA can be physically crosslinked via freeze–thaw cycles, avoiding toxic chemical agents and enabling control over porosity and elasticity. Chitosan, a cationic polysaccharide, is biodegradable, non-toxic, and exhibits antimicrobial action by disrupting microbial membranes [16–18]. Additionally, it promotes wound healing by facilitating cell migration and proliferation [19].

In contrast with PVA and chitosan, casein, a milk derived protein, has been less explored to produce wound dressings, but it recently gained interest due to its ability to origin bioactive peptides upon enzymatic hydrolysis [20,21]. These peptides present antioxidant properties that help regulate the oxidative environment in wounds, thereby reducing cellular damage and promoting tissue repair; this is particularly important in diabetic wounds where oxidative stress can impair healing [22,23]. The peptides also contribute to maintaining the wound site free from pathogens due to their antibacterial properties [24]. Furthermore, casein has moderate antioxidant capacity by itself due to the presence of amino acids, which may be involved in radical scavenging [25].

To further enhance the therapeutic performance of the hydrogels, bioactive agents like ozonized oils and astaxanthin, with well-documented antioxidant and antimicrobial properties, can be added to the formulations. Ozonized oils exhibit strong antimicrobial activity through the release of ozone that disrupts bacterial membranes [26–28]. They also promote oxygenation of the wound site, supporting metabolic processes essential for tissue repair, and have demonstrated biofilm disruption capabilities, particularly in antibiotic-resistant infections. Astaxanthin (Fig. 1C) is a potent lipophilic carotenoid with high free radical scavenging capacity and anti-inflammatory properties. It accelerates wound closure by reducing oxidative damage, promoting collagen organization, and supporting cell proliferation [29–31].

The objective of this work was to produce PVA/chitosan/casein hydrogels containing different amounts of ozonized oils or astaxanthin and test their biomedical properties. We hypothesized that the integration of casein with these bioactive agents would synergistically improve the antioxidant and antimicrobial performance of the hydrogel dressings while maintaining adequate mechanical and biological properties for wound application. To test this hypothesis, a comprehensive physicochemical and biological characterization was performed, covering antioxidant capacity, swelling behavior, mechanical and rheological properties, mucoadhesion, cytocompatibility, hemocompatibility, and antibacterial activity.

2. Materials and methods

2.1. Materials

PVA (MW146000-180000) and casein sodium salt were purchased from Sigma. Low molecular weight chitosan (deacetylation degree 76 %) was provided by Bioceramed. Triethanolamine was purchased from PanReac AppliChem and acetic acid from Fisher Chemical. Lysozyme (from chicken egg white, 40,000 units/mg protein) was from Sigma. To simulate an exudate solution, a pseudo extracellular fluid (PECF) was prepared using distilled and deionized (DD) water and 6.8 g/L NaCl (Sigma), 2.29 g/L KCl (Sigma), 2.5 g/L $NaHCO_3$ (PanReac AppliChem) and 4.0 g/L NaH_2PO_4 (Sigma). DD water (18 MΩ cm) was obtained from a Millipore Milli-Q® system. Phosphate buffered saline (PBS, pH of 7.4 at 25 °C) was prepared using tablets purchased from Sigma that were dissolved in DD water. Astaxanthin and dimethyl sulfoxide (DMSO) were purchased from Sigma, as well as 2,2- diphenyl-1-(2,4,6-trinitrophenyl) hydrazin-1-yl (DPPH) for the antioxidant tests. Three ozonized oils from PeroxiBiokey, containing different proportions of sunflower (Helianthus annus) and olive oil (Olea europaea), and characterized by different peroxide values[1] were used: one with the volume ratio 85:15 (sunflower: olive oil) and 1200 meq O_2/kg, another equivalent but partially deodorized and finally one with the ratio 50:50 (sunflower: olive oil) and 800 meq O_2/kg.

For the cytotoxicity assay, NIH/3T3 fibroblasts were purchased from ATCC®, Dulbecco's modified eagle's medium (DMEM), bovine fetal serum, penicillin-streptomycin solution, and trypsin-EDTA (ethylenediaminetetraacetic) were purchased from Sigma. Brain Heart Infusion (BHI) agar and Mueller-Hinton agar used for the antimicrobial tests were purchased from Oxoid.

2.2. Preparation of the hydrogels

The base hydrogel (B) was prepared using the FT method combining PVA, casein, and chitosan in a final polymer mass ratio of 60:20:20 (w/w). This ratio was preserved across all formulations, irrespective of the incorporated bioactive agents, and was previously optimized to balance mechanical integrity, porosity, and peptide release (preliminary tests not shown). A solution of 5 % (w/v) of PVA was prepared by dissolving 0.5 g of PVA in 10 mL of DD water at 90 °C in an oven overnight. Solutions of 2.5 % (w/v) chitosan and 16 % (w/v) casein were also prepared. For the chitosan solution, 136 μL of acetic acid was dissolved in 6.66 mL of DD water (corresponding to a final concentration of ~2 % (v/v)). The mixture, with a final pH of ~4.5, was then vigorously stirred with 0.17 g of chitosan until complete dispersion. The casein solution was prepared by adding 0.17 g of casein to 1.02 mL of DD water previously mixed with 43 μL of triethanolamine, under magnetic stirring. The final pH of the solution was ~7.6. The casein solution was added to the PVA solution and stirred until homogeneity was reached. The resulting solution was thereafter mixed with the chitosan solution. The final solution was poured into petri dishes, and the sequence of FT cycles was initiated. Those consisted of 5 cycles, each with 23 h at −20 °C and 1 h at room temperature.

Six hydrogels containing active agents (astaxanthin and ozonized oils), keeping a constant PVA/chitosan/casein ratio, were produced (see Table 1).

For the astaxanthin dressings, solutions of astaxanthin were prepared by dissolution in 500 μL of DMSO and subsequently added to the PVA solution and mixed for over 1 h, prior to the homogenization step with the casein solution. Two concentrations of astaxanthin were considered giving rise to hydrogels BAx_1 and BAx_2.

Regarding ozonized oils, they were added to the casein solution and stirred for 1 h, being the remaining procedure identical to the one described above. To evaluate the effect of the degree of ozonation (1200 and 800 meq O_2/kg), two distinct oils were used to obtain BOz12_2 and BOz8_2 hydrogels. Samples were prepared with different contents of the same ozonized oil (BOz12_1 and BOz12_2). Finally, a partially deodorized oil was used to prepare the sample BOzD12_2. A scheme that resumes the preparation procedure is presented in Fig. 2.

Following the FT cycles, all hydrogels were washed by immersion in DD water for 24 h to eliminate reagents that were not bonded to the polymeric matrix. After that, the hydrogels were stored in the hydrated state inside sealed containers in the refrigerator at 4 °C. Before the characterization assays, discs with proper dimensions were cut from the hydrogel's plates using circular punchers (typically with diameter of 10 mm, thickness 2–3 mm and average hydrated mass of 35 mg, unless otherwise stated).

[1] The peroxide value measures the amount of peroxidic species formed during the ozonation process and is expressed in meq O_2/kg, referring to the amount of oxygen bound in peroxide groups (O–O bonds).

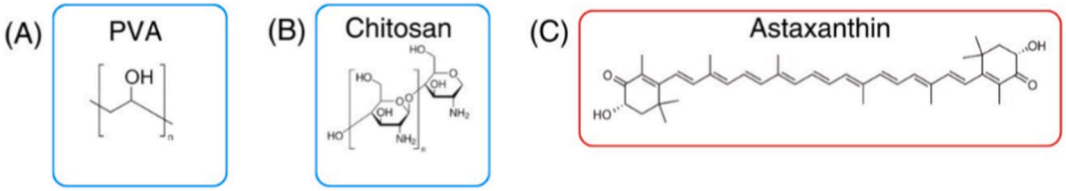

Fig. 1. Chemical structures of (A) PVA, (B) chitosan and (C) astaxanthin. The structures of casein and ozonized oils are not shown because both are complex mixtures.

Table 1
Compositions of the produced hydrogels.

Code Name	PVA (mg)	Chitosan (mg)	Casein (mg)	Astaxanthin (mg)	Ozonized oil (mg)
B	500	170	170	0	0
BAx_1	500	170	170	16.8	0
BAx_2	500	170	170	33.6	0
BOz12_1	500	170	170	0	250[a]
BOz12_2	500	170	170	0	500[a]
BOzD12_2	500	170	170	0	500[b]
BOz8_2	500	170	170	0	500[c]

[a] Ozonized oil with 1200 meq O_2/kg.
[b] Ozonized oil with 1200 meq O_2/kg partially deodorized.
[c] Ozonized oil with 800 meq O_2/kg.

2.3. Characterization of the hydrogels

2.3.1. Antioxidant capacity

For the determination of antioxidant capacity, the DPPH assay was used, due to its simplicity and peed [32]. The radical DPPH was dissolved in ethanol to obtain a 90 μM solution. The hydrogel discs were immersed in 400 μL of the DPPH solution and then incubated in the dark, at room temperature, for 30 min. After incubation, the absorbance of the supernatant from each sample was measured at 517 nm using a Multiskan™ GO Microplate spectrophotometer (Thermo Fisher Scientific, Kandel, Germany). The antioxidant activity was calculated using equation (1):

$$DPPH\ Inhibition\ (\%) = \frac{A_c - A_s}{A_c} \times 100, \quad (1)$$

where A_c is the absorbance of the control (400 μL DPPH solution without sample immersion) and A_s is the absorbance of the supernatant. Experiments were performed in triplicate.

2.3.2. Morphology

Analysis of the hydrogel morphology was carried out using a Scanning Electron Microscope Hiitachi S-2400 with an accelerated voltage of 10 kV. Hydrogel discs were immersed in liquid nitrogen for 20 s, fractured in half and lyophilized for 16 h using a freeze-dryer (Alpha 1–2 LDPlus, Germany). Prior to SEM observation, all discs were sputter-coated with a conductive layer of gold:palladium (20:80) using a turbo-pumped sputter coater (Q150T ES Quorum, UK). Both surfaces and cross-sections were observed.

2.3.3. Chemical structure

The chemical structure of the hydrogels was studied by Fourier-transform infrared spectroscopy (FTIR-ATR) using a Spectrum Two™ (PerkinElmer, Waltham, MA, USA) equipped with a PerkinElmer Universal Attenuated Total Reflectance (UATR) Two Accessory. Prior to the measurements, discs of each hydrogel were dried in a vacuum oven at 45 °C for 24 h. The spectra were then acquired in the range of 4000 - 400 cm^{-1}, with a resolution of 4 cm^{-1}. After acquisition, the spectra were normalized and analyzed using OriginPro 2016 software. Three measurements were carried out for each formulation.

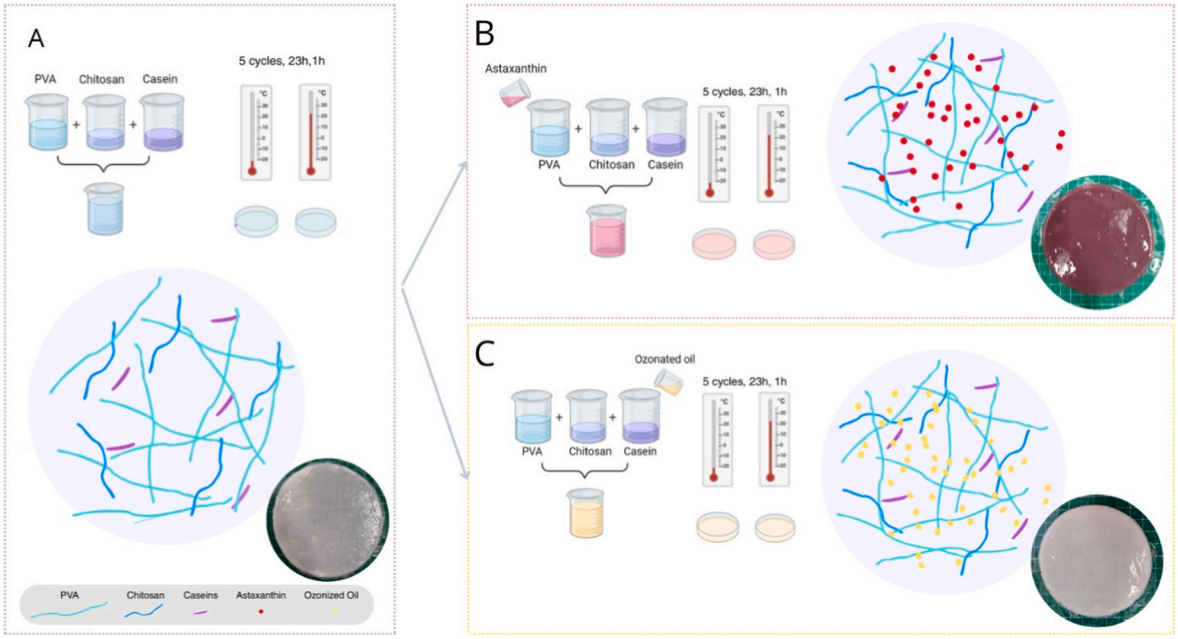

Fig. 2. Scheme of the hydrogel's preparation procedure. Photos of the obtained materials in their final state (hydrated) are included.

2.3.4. Wettability

The captive bubble method was used to measure the water contact angles in the different materials. Images of the bubbles generated with an inverted syringe under the bottom face of the hydrogel discs were captured for 30 s after bubble deposition using a video camera (jAi CV-A50, Spain) connected to an optical microscope (Wild M3Z, Leica, Germany) coupled to a frame grabber (DT3155 Data Translation, Norton). The determination of the contact angles was performed using ADSA-P software (Axisymmetric Drop Shape Analysis – Profile, Canada). More than 7 independent measurements were conducted for each material.

2.3.5. Equilibrium water content

To conduct the water content assay, discs of each formulation (in triplicate) were weighed using a semi-micro analytical balance. Subsequently, the discs were dried in a vacuum oven at 45 °C for 24 h and then reweighed. The equilibrium water content (EWC) was calculated using equation (2):

$$EWC(\%) = \frac{W_H - W_D}{W_H} \times 100. \quad (2)$$

where W_H is the weight of the hydrated discs and W_D is the weight of the dry discs.

2.3.6. Water vapor transmission rate

The water vapor transmission rate (WVTR) of the hydrogels was analyzed following ASTM standard E96-95 [33]. Hydrogel discs were clamped between the chambers of a Franz cell previously filled with DD water. The entire system was weighed and subsequently placed in a humidity chamber at 32 °C and 50 % humidity for 24 h. After that period, the system was weighed and the WVTR calculated by equation (3):

$$WVTR\ \left(g.m^{-2}.24h^{-1}\right) = \frac{\left(W_i - W_f\right)}{A \times t} \times 24, \quad (3)$$

where W_i and W_f are the initial and final weights, respectively. A is the area of hydrogel in contact with both water and air, and t is the duration of the experiment. The assays were done in triplicate.

2.3.7. Degradation

Hydrogel discs were dried in a vacuum oven at 45 °C for 24 h, weighed (W_0) and incubated in 1 mL of degradation solution, at 34 °C with agitation (180 rpm). In the enzymatic degradation studies, PECF with 1 mg/mL of lysozyme was used, while hydrolytic degradation was carried out in PBS. After 24 and 48 h, the discs were removed from the solutions, washed by immersion in DD water (50 mL per disc of 10 mL diameter) during 24, with renewal by fresh water after 12 h, to remove soluble salts, and dried again following the initial procedure. The final weights of the discs were recorded ($W_{24/48}$). The test was performed in triplicate and the resultant weight loss was calculated through equation (4):

$$Weight\ loss\ (\%) = \frac{W_0 - W_{24/48}}{W_0} \times 100. \quad (4)$$

2.3.8. Tensile behavior

Tensile tests were performed using a TA. XT Express Texture Analyzer (Stable Micro Systems, UK) equipped with a 50 N load cell. The tests were carried out at room temperature using hydrated hydrogel samples with a dumbbell shape (10 mm gauge and 2.5 mm width). Each sample was subjected to a strain rate of 0.5 mm/s till rupture. The elasticity modulus and failure strain of the hydrogels were determined from the stress strain curves. The tests were done in quadruplicate for each hydrogel formulation.

2.3.9. Rheological behavior

Rheological measurements were performed using a Modular Compact Rheometer (MCR-92, Anton Paar, Austria) at 37 °C with a parallel measuring plate (PP25). The hydrogel discs (25 mm in diameter) were placed between the plates and compressed by 2 % of their thickness while being surrounded by DD water. To determine the linear viscoelastic region, amplitude sweeps were performed in a range of shear strain from 0.01 % to 100 % at a constant angular frequency of 10 rad/s. After that, oscillatory frequency sweep tests were conducted upon the hydrogels in a range from 0.1 rad/s to 100 rad/s at a constant amplitude strain (0.1 %) obtained from the previous amplitude sweeps. During these tests, both the loss (G'') and storage (G') moduli were obtained. The loss tangent was calculated through equation (5):

$$tan\ \delta = \frac{G''}{G'}. \quad (5)$$

2.3.10. Mucoadhesion

Mucoadhesion testing was conducted using a TA. XT Express Texture Analyzer (Stable Micro Systems, UK). Hydrogel discs were glued to the superior moving probe and brought into contact with a sample of large intestine porcine mucosa securely held in a cylindrical holder fixed in the bottom of the equipment. The moving probe with the glued hydrogel established contact with the mucosa for 10 s and was then withdrawn at a constant velocity of 0.05 mm/s. The maximum detachment force required for separating the hydrogel from the pig mucosa was registered and the work of adhesion was calculated from the area under the curve force *vs* distance. At least three measurements were performed per formulation.

2.3.11. Biological activity

2.3.11.1. Irritability. Hen's Egg Test – Chorioallantoic Membrane (HET-CAM) was performed following the recommended protocol [34] to evaluate potential irritating effect of hydrogels. Fertilized chicken eggs were incubated at 37 °C and 60 % humidity for 8 days in an incubator (YZ-56S, China). On the ninth day, the upper shell of the eggs was cut with a rotary saw (Dremel 3000 from Breda, Netherlands), and the exposed inner membrane was hydrated with 0.9 % (w/v) NaCl solution. Thirty minutes after the solution was decanted, and the inner membrane removed to expose the CAM. The hydrogel discs were placed directly on top of the CAM. The appearance of CAM was monitored for 5 min, to observe eventual signs of hemorrhage, lysis or coagulation. Negative and positive controls were prepared with 0.9 % (w/v) NaCl and 0.1 M NaOH, respectively. The irritation score was calculated according to Ref. [35]. Three tests were performed for each formulation.

2.3.11.2. Hemocompatibility. The hemocompatibility of the hydrogels was evaluated using the ASTM F756-17 standard [36]. Blood samples were collected from healthy volunteers, with informed consent (approval by the Ethical Committee of Egas Moniz, Ref. n◦1047/2022), at the Health Service of Instituto Superior Técnico. Hydrogel discs were immersed in 5 mL of PBS in a 15 mL falcon. After adding 200 μL of blood, the falcons were closed and incubated for 1 h at 37 °C. Finally, the discs were removed from the solutions, which were centrifuged for 10 min at 3000 rpm. Positive and negative controls were prepared following the same procedure but adding the blood only to DD water and PBS, respectively. The absorbance of the supernatant was measured in a UV/Vis spectrophotometer (Thermo Fisher Multiskan GO, USA) at 540 nm, and the hemolysis ratio (HR) calculated through equation (6):

$$HR\ (\%) = \frac{A_s - A_{nc}}{A_{pc} - A_{nc}} \times 100, \quad (6)$$

where A_s is the absorbance of the supernatant in which the sample was immersed, and A_{nc} and A_{pc} are the absorbances of the negative and

positive controls, respectively.

2.3.11.3. Cytotoxicity. The cytotoxicity of the hydrogels was evaluated following the standard protocol described in Ref. [37]. Before the assays, the hydrogel discs were sterilized inside a laminar flow cabinet (Bio Air Instruments, model AURA 2000 MAC 4 NF), by immersing the samples in 70 % (v/v) ethanol for 1 min and then in sterile DD water.

NIH/3T3 fibroblasts (Sigma) were seeded in 12-well plates (approximately 1×10^5 cells/well) in DMEM (Dulbecco's Modified Eagle Medium) that has been supplemented with 10 % (v/v) fetal bovine serum and 1 % (v/v) penicillin-streptomycin solution. The plates were then incubated at 37 °C in a humidified atmosphere with 5 % CO_2, for 24 h. After this period, the culture medium was replaced by fresh medium, and the discs were placed in the Transwell® inserts. Additional 200 μL of medium were added to the hydrogels, which were then incubated for further 24 h. Four replicates for each hydrogel type were considered. In addition to the experimental groups, a negative control (DMEM) and a positive control with 10 % DMSO in culture medium were also included. To perform the MTT assay, the inserts with the discs and the medium were removed and the wells were washed with PBS. Next, the MTT solution (0.5 mg/mL MTT in serum-free DMEM) was added to the wells and incubated for 3 h. To dissolve the formazan crystals, isopropanol solvent (0.1 % V/V IGEPAL in isopropanol with 4 mM HCl) was added. Finally, the absorbance was measured using a microplate reader (Infinite 200Pro, Tecan) at 565 nm, and the cell viability was calculated using equation (7), where A_s and A_{nc} are the normalized values of the absorbance of the samples and negative controls, respectively.

$$\textit{Cell viability}\ (\%) = \frac{A_s}{A_{nc}} \times 100. \tag{7}$$

2.3.11.4. Antibacterial properties. The antibacterial activity was assessed by the Kirby-Bauer disc diffusion assay (or agar diffusion assay). In total, 20 bacterial strains with different resistance to antibiotics were used: 5 vancomycin-susceptible *Enterococcus faecium*, 5 vancomycin-resistant *Enterococcus faecium* (VRE), 5 *Escherichia coli*, and 5 extended-spectrum beta-lactamases (ESBL) *Escherichia coli*.

All strains were grown in BHI for 24 h at 37 °C. Subsequently, a turbidity equivalent to 0.5 McFarland (1.5×10^8 bacteria/mL) was prepared for each bacterium. The inoculum was then seeded onto Mueller-Hinton agar plates. Hydrogel discs of 4 mm diameter, sterilized according to the procedure mentioned in the previous section, were placed on the inoculated agar and incubated for 18–24 h at 37 °C. Positive controls (standard antibiotic discs) and negative controls (blank hydrogel discs) were included for comparison. Finally, the diameter of the halos (if present) was measured using a caliper. Three replicates were done for each system. It shall be noted that, due to the low aqueous solubility of some active agents (e.g., astaxanthin and ozonized oils), the disc diffusion assay may underestimate the antimicrobial activity of the formulations.

2.4. Statistical analysis

Statistical analysis was performed using GraphPad Prism software (version 9.0). Data are presented as mean ± standard deviation. The Shapiro-Wilk test was used to assess the normality of the results. For datasets following normal distribution, one-way ANOVA was carried out for multiple comparisons, and Student t-test was used to compare two groups. When data did not follow a normal distribution, the Mann-Whitney test was employed to compare two independent groups. A significance threshold was set at 0.05. Statistical differences are marked with asterisks, where * indicates $p < 0.05$, ** indicates $p < 0.005$, and *** indicates $p < 0.0005$.

3. Results and discussion

3.1. Antioxidant capacity

The DPPH assay was performed to determine the antioxidant activity of the prepared hydrogels. The results (Fig. 3) show that all hydrogels present antioxidant activity, including the base hydrogel (B). This could be associated with the reported antioxidant activity of the main components of the hydrogel matrix (namely casein and chitosan). Casein contains specific amino acid residues, such as tyrosine, tryptophan, cysteine, and histidine, which can donate electrons or hydrogen atoms, neutralizing free radicals [25]. The antioxidant properties of chitosan depend on factors like molecular weight and degree of deacetylation. Anraku et al. [38] reported that chitosan with low molecular weight and a high degree of deacetylation exhibits enhanced antioxidant activity. This activity is attributed to chitosan's ability to scavenge free radicals (such as hydroxyl and superoxide radicals) through the reactive hydroxyl and amino groups present in its molecular structure.

The incorporation of the active agents improved the antioxidant response of the hydrogel. *Regarding astaxanthin, BAx_1 increased the antioxidant activity of the hydrogel by 53 % compared with hydrogel B ($p = 0.0238$). Doubling the amount of astaxanthin (BAx_2) led to an additional 15 % increase ($p = 0.0428$), indicating a saturation effect.* Due to their hydrophobic nature, astaxanthin molecules tend to aggregate, particularly at high concentrations. These aggregates can cause steric hindrance, limiting the accessibility of active sites and thereby reducing their effectiveness in scavenging free radicals [39,40]. Additionally, astaxanthin can interact with the components of the hydrogel (chitosan and casein), which may decrease the availability of active sites and consequently its antioxidant activity.

In the case of ozonized oils, the hydrogel BOz12_1 (1200 meq O_2/kg) increased antioxidant activity by 49 % ($p = 0.0262$), while doubling the amount of the same oil (BOz12_2) further enhanced activity by 71 %. These results confirm the dose-dependent effect of both bioactive agents, although saturation occurred earlier for astaxanthin than for ozonized oil. Similar results were reported by Cho et al. [41], who found, through DPPH assays, that ozonized sunflower oil has a potent dose-dependent radical scavenging activity. The antioxidant activity of ozonized vegetable oils results from the presence of powerful natural

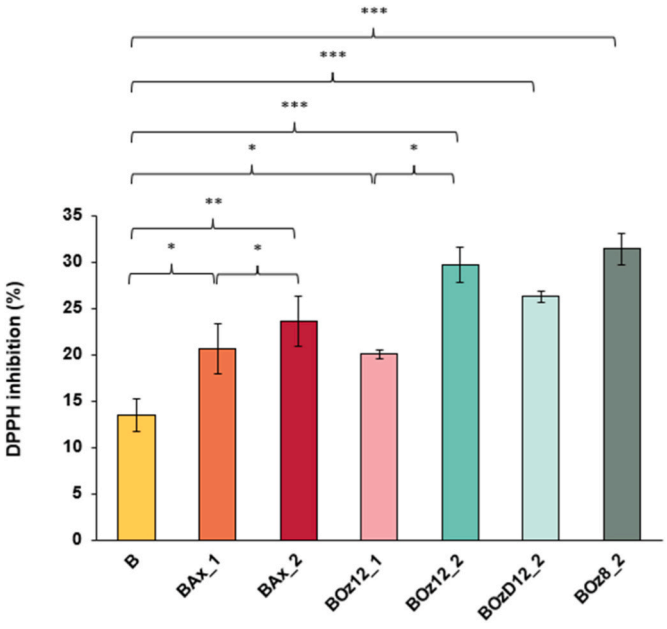

Fig. 3. Antioxidant capacity of hydrogels. The error bars represent the ±mean standard deviations (n = 3).

antioxidants, like polyphenols and tocopherols (quite abundant in olive oil [42]and sunflower oil [43], respectively), but may also be due to the formation of ozonides (secondary antioxidants) when ozone reacts with unsaturated fatty acids present in the oils [44]. The results obtained in the present work suggest that further increasing the concentration of the oil could improve even more the antioxidant activity. This was attempted, but higher amounts of oil resulted in phase separation, originating hydrogels comprising a solid matrix with a visible oil film on the surface.

The presence of certain volatile compounds (e.g. aldehydes, ketones, and free fatty acids) in the ozonized oils may confer them an undesirable smell. A deodorization process, involving steam distillation at high temperature under vacuum, is often used to eliminate these compounds and turn the oil more appealing. The high temperatures associated with the process can degrade sensitive components, including the antioxidants (e.g., polyphenols and tocopherols) [45]. Therefore, the hydrogel prepared with deodorized ozonized oil (BOzD12_2) was compared to the equivalent one containing the non-deodorized oil (BOz12_2). The results showed that the odour removal process led to a slight reduction of the DPPH inhibition power from 29.7 % to 26.3 %, nevertheless it was not statistically significant ($p = 0.0684$).

Finally, a third oil, with a higher content of olive oil (volumetric ratio sunflower oil:olive oil 50:50) and a lower peroxide value (800 meq O_2/kg) was used to produce the hydrogel BOz8_2 and the results were compared to those obtained for BOz12_2, which contains the same amount of ozonized oil but with the ratio 85:15 and a peroxide value 1200 meq O_2/kg. A slightly higher DPPH inhibition percentage was observed for BOz8_2 (31.4 %), but the difference to BOz12_2 was not statistically significant ($p = 0.3880$). It is known that the antioxidant activity increases when peroxide values decrease [46] still the differences in oil composition can mask this effect. In fact, the ozonation of vegetable oils is a complex process that depends on various factors, including the processing conditions and the type of oil. Ozone is a strong oxidizing agent that may react with polyphenols and tocopherols of vegetable oils, reducing their concentration and antioxidant effectiveness. Besides, it may interact with the double bonds of unsaturated fatty acids, leading to the formation of new compounds (peroxides, aldehydes, and carboxylic acids) [47] that may also affect the antioxidant capacity of the oils.

Based on the obtained results, four hydrogels were chosen for a more detailed characterization, and compared to hydrogel B: BAx_1 and BAx_2 to evaluate the effect of the concentration of this carotenoid on other properties, and BOz8_2 and BOz12_2, since they exhibited the highest antioxidant activities.

3.2. Morphology

SEM images of the surface and cross-section of the selected hydrogels are depicted in Fig. 4 and show that all hydrogels have a porous structure, which is typical for PVA hydrogels produced by FT [48]. During the freezing step, ice crystals form and repel PVA chains leading to a PVA-rich phase that enhances the formation of polymeric crystallites. Upon thawing, the ice melts leading to the formation of pores, while crystallites keep their integrity. Increasing the number of FT cycles promotes the establishment of hydrogen bonds between the polymer chains and increases the crystallinity degree, contributing to a stable and robust network architecture. This results in the formation of an insoluble hydrogel with a semicrystalline structure, displaying localized regions of crystallites dispersed in an amorphous polymer matrix [49].

For hydrogel B, interconnected pores are especially evident in the image of the cross-section. The addition of astaxanthin led to changes in the morphology of the hydrogel: BAx_1 presents a more irregular and porous surface and a cross-section with a fibrous-like porous structure. Doubling the quantity of astaxanthin (BAx_2) led to a more compact structure, where pores remain visible and more uniformly distributed. The hydrogels containing ozonized oils are slightly different: the structure of BOz8_2 resembles that of hydrogel B both in surface and cross-section; BOz12_2 presents smaller features and a lower bulk porosity.

3.3. Chemical structure

The chemical composition of the hydrogels was analyzed using infrared spectroscopy, and the normalized spectra are displayed in Fig. 5. Additionally, Fig. S1 in Supplementary Information shows the spectra of the components used in the production of the hydrogels.

A broad band (highlighted in grey in the figure) was detected in all hydrogels with the center peak near 3285 cm^{-1}, typically corresponding to O–H stretching. This band is commonly found in PVA due to the hydroxyl group of the alcohol in its structure and the presence of some residual water, which remained after the drying process. The band around 2940-2907 cm^{-1} (highlighted in yellow), which is present in all spectra, is related to the stretching vibration of C–H present in PVA, chitosan and the oils. These peaks are more pronounced in spectra of the hydrogels containing oils, which is consistent with the high intensity of the same peaks in the pure components (oil 1200 and oil 800) shown in Fig. S1. The PVA spectrum presents also two characteristic peaks at ≈1140 cm^{-1} (C–O stretching) and ≈1080 cm^{-1} (C═O stretching) (Fig. S1), related to the crystalline and amorphous phases, respectively [50]. Both peaks were detected in the spectra of all hydrogels (highlighted in orange), and the decrease in the transmittance ratio 1140/1080 observed for B, BAx_1, and BAx_2 suggests a lower crystallinity degree compared with that of BOz12_2 and BOz8_2 [50]. However, the presence of chitosan with a typical peak around 1150 cm^{-1} (Fig. S1), which derives from asymmetric stretching of the C–O–C bridge in Ref. [51], may interfere with those results. The same peak appears in the spectra of ozonized oils [52] In the same spectral region, peaks at 1066 and 1028 cm^{-1} are typically seen in the spectrum of chitosan, which are assigned to C–O stretching [51]. These peaks may be detected in the spectrum of hydrogel B (highlighted in orange), but they overlap with different peaks in the spectra of the other hydrogels.

The molecular structures of caseins include several amine groups. The main characteristic peaks seen in their spectrum are 1516 cm^{-1} deriving from the stretching vibration of C–N and bending of N–H, and 1664 cm^{-1} assigned to carbonyl groups (Fig. S1) [53]. These peaks (highlighted in blue) were clearly detected in the spectra of all hydrogels.

At 3009 cm^{-1}, a low intensity peak (highlighted in green) correspondent to C–H stretching vibration of the *cis*-double bond (=C–H) was observed in the spectra of BOz8_2 and BOz12_2. This peak is characteristic of ozonized oils (Fig. S1) [52]. In the region 2940 cm^{-1} to 2907 cm^{-1} (stretching vibration of C–H in PVA), the spectra of hydrogels BOz8_2 and BOz12_2 show stronger peaks (2960 - 2850 cm^{-1}) due to vibration of the aliphatic groups (CH3 and CH2 respectively) existent in ozonized oils [54]. Another characteristic peak of the oils may be seen in the spectra of BOz8_ and BOz12_2 at 1740 cm^{-1} (highlighted in purple), deriving from the carbonyl groups [55]. It became more intense in BOz12_2 than BOz8_2, reflecting the increase of the carbonyl content in the oil with higher degree of ozonation.

The spectrum of astaxanthin presents several peaks between 1651 cm^{-1} and 960 cm^{-1} (Fig. S1), which are superimposed to the peaks of other components of the hydrogels. However, it is possible to observe on the spectra of hydrogels containing astaxanthin, BAx_1 and BAx_2, a slight enhancement of the peak at 1550 cm^{-1}, corresponding to stretching vibration of C═C in astaxanthin [44].

Overall, the hydrogel network formation shall be primarily driven by non-covalent interactions, including hydrogen bonding, electrostatic interactions, hydrophobic interactions, and van der Waals forces. PVA has a high number of hydroxyl groups that can form strong hydrogen bonds with amino and hydroxyl groups of chitosan and casein; electrostatic interactions are expected to establish between the positively charged amino groups of chitosan and negatively charged groups of

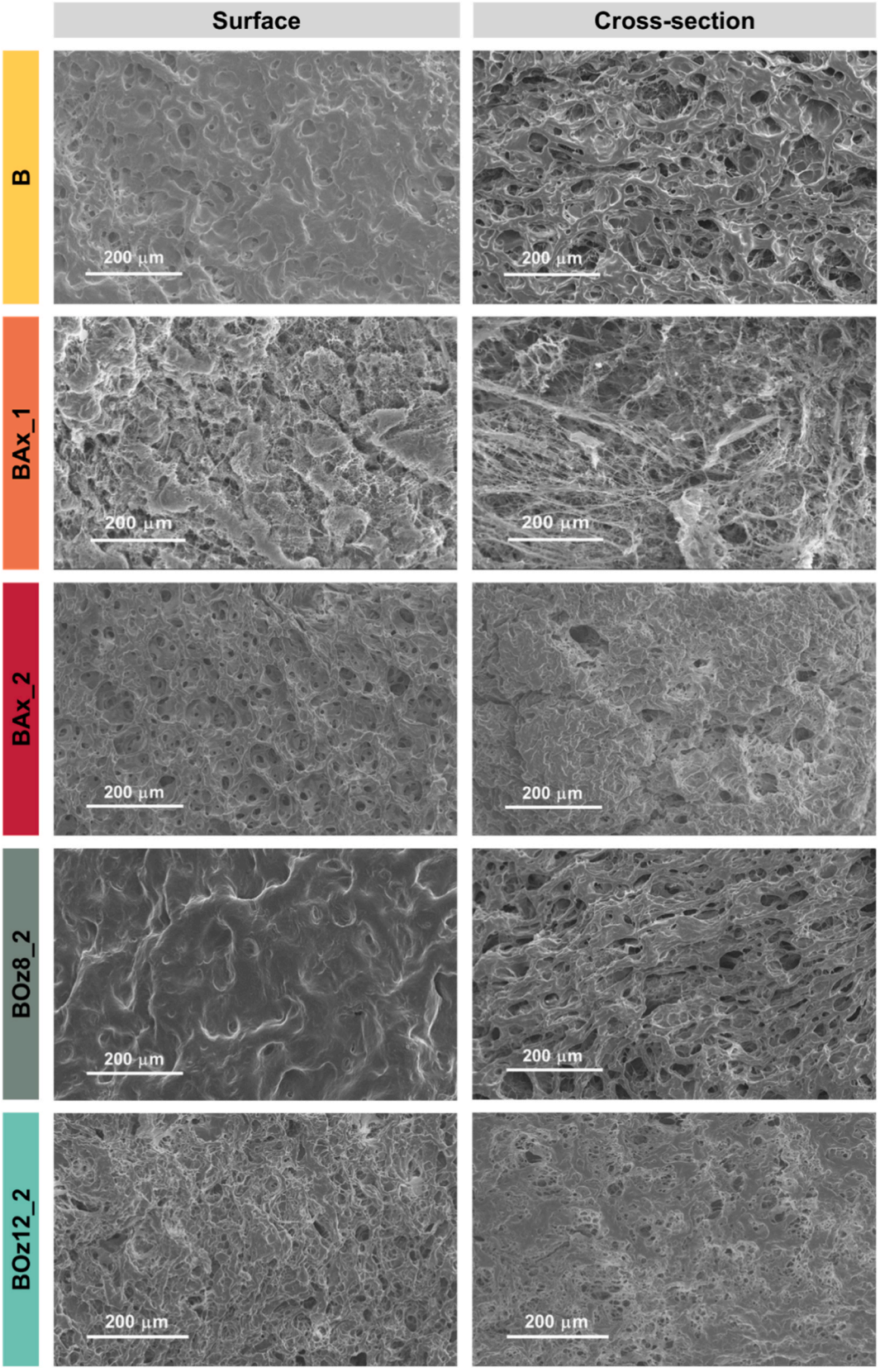

Fig. 4. SEM images of the hydrogels surface and cross-section.

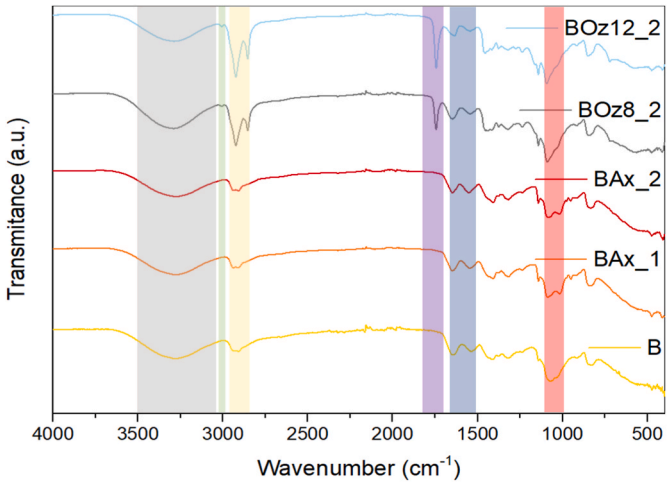

Fig. 5. FTIR-ATR spectra (4000–400 cm^{-1}) of hydrogels with highlights of specific bands.

casein (e.g., carboxylates or phosphates); hydrophobic interactions shall occur between non-polar amino acid residues in casein stabilizing the hydrogel structure. During freeze-thawing cycles, PVA undergoes physical crosslinking through the formation of crystalline domains, which also enhances the mechanical integrity of the hydrogel. The increase in viscosity inherent to this process reduces the mobility of casein molecules in the formulation, hindering the dynamic assembly behavior required for micellization. Micelle formation is also impaired by the interactions between casein and PVA or chitosan, which compete with casein-casein associations. Finally, the use of casein sodium salt, a soluble de-micellated form of casein, to prepare the hydrogel shall contribute to prevent micelle formation, as it is unable to self-assemble in the absence of calcium and phosphate ions [56].

When astaxanthin or ozonized oils are incorporated into the hydrogel, they shall also interact with the polymer network primarily through non-covalent interactions, such as hydrogen bonding (between hydroxyl and carbonyl groups), hydrophobic interactions (with non-polar regions of casein and chitosan), and, in the case of astaxanthin, possible π–π stacking. Ozonized oils may also form weak electrostatic interactions if carboxylic acid groups are present and ionized. These interactions help retain the bioactive compounds within the hydrogel and contribute to its structural stability and antioxidant functionality.

3.4. Wettability

Fig. 6 shows that all hydrogels are hydrophilic, presenting values of water contact angles between 44° and 55°. The incorporation of astaxanthin slightly increased the average value of the contact angle, while ozonized oil with 800 meq O_2/kg led to a decrease and ozonized oil with 1200 meq O_2/kg had practically no effect on the wettability. Yet, none of the variations were statistically significant. The hydrophilic nature of the produced materials results from the presence of hydroxyl groups (-OH) in PVA, casein, and chitosan, amine groups (-NH_2 and = NH) in chitosan and casein, and phosphate groups (-PO_4) in casein. Hydrophilic materials are ideal for exudative wounds due to their ability to absorb water and promote faster healing [57]. However, these materials present challenges, particularly during dressing removal. When a clot forms between the dressing and the wound tissue, removing the dressing requires extreme care to minimize the chances of its disrupting [58].

3.5. Equilibrium water content

The produced hydrogels presented a significantly high value of EWC (Fig. 7), which is critical to maintain a moist wound environment, support debridement and minimize pain, thus benefiting wound healing. The water retention of the hydrogels is associated with their hydrophilic character and their porosity. Although both astaxanthin and the ozonized oils are hydrophobic, their incorporation in the hydrogels led to an increase in the EWC, which was slightly more accentuated in the case of astaxanthin: maximum of 5.4 % increase for Bax_2 relative to hydrogel B. The observed increase may be related to different pore morphologies, as depicted in Fig. 4. It must be stressed that the lyophilization process undergone by the hydrogels before SEM analysis may affect the porous structure in different ways, depending on their composition. Thus, direct correlations between the SEM images and the EWC values may not be obvious.

Moreover, the addition of drug molecules prior to FT may interfere with the formation of physical crosslinks affecting the production of more crystalline zones, potentially altering the overall hydrogel network, which could change the swelling behavior of the materials. This has been seen previously for PVA based hydrogels with addition of chitosan [59] and drug molecules [60,61] On the other hand, the presence of drug molecules can also lead to a promotion in crystalline sites or increase in physical links [62].

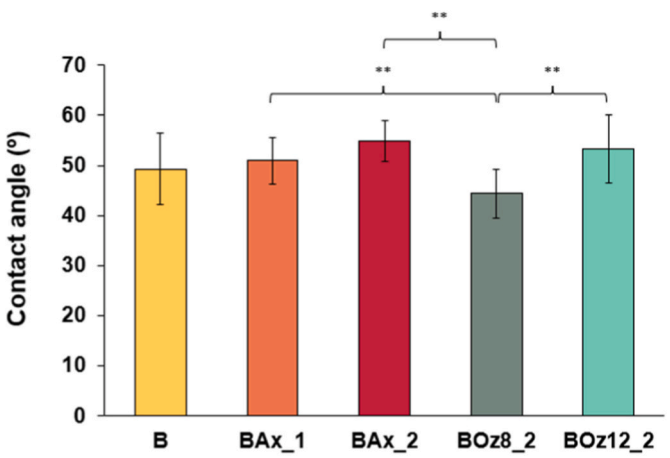

Fig. 6. Water contact angle of the hydrogels. The error bars represent the ±mean standard deviations.

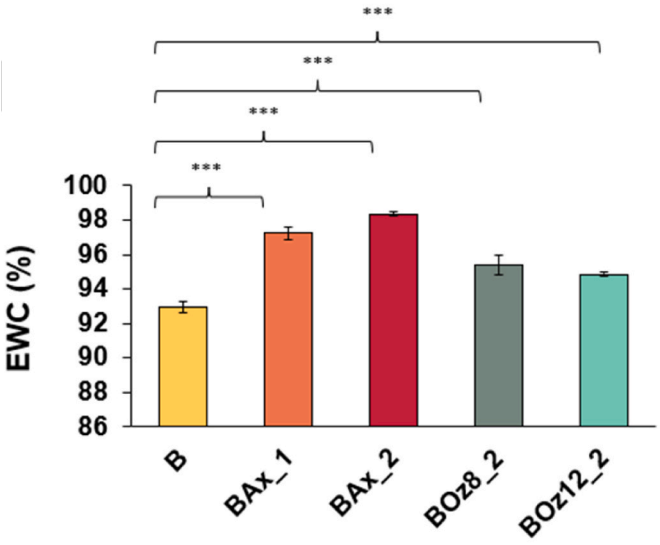

Fig. 7. EWC (%) of the hydrogels. The error bars represent the ±mean standard deviations.

3.6. Water vapor transmission rate

The WVTR of a dressing applied on the wound influences its level of moisture, consequently it affects the wound healing process. Whereas dressings with high WVTR may lead to dehydration of the wound, low WVTR dressings could be responsible for maceration of the skin due to accumulation of wound fluid. Therefore, different wounds require different conditions of moisture. Accordingly, an ideal dressing should have a transmission rate at least higher than the WVTR of normal skin [63] (on average 204 ± 12 g m^{-2}.24 h^{-1} [64]).

Hydrogels are materials known for their high values of WVTR. Fig. 8 displays the WVTR values for the tested hydrogels, ranging from 3877 ± 858 g m^{-2}.24 h^{-1} to 10145 ± 1059 g m^{-2}.24 h^{-1}. The hydrogels containing astaxanthin have the highest WVTR values.

As previously mentioned, excessively high WVTR may lead to dehydration of the wound surface. A suitable range of permeability to moisture vapor in commercial wound dressings lies between 76 g m^{-2}.24 h^{-1} and 9360 g m^{-2}.24 h^{-1}, according to the clinical needs [65]. Wu et al. [66] studied the water vapor loss characteristics of some hydrogel dressings and found their WVTR to be above 9000 g m^{-2}.24 h^{-1}.

The results indicate that all hydrogels, except BAx_2, presented adequate WVTR values. However, in clinical practice, the high WVTR of some hydrogels can be managed by using a self-adhesive fabric cover, like Mefix®, as suggested by Queen et al. [67]. Thus, hydrogel BAx_2 would require additional covering to effectively control its WVTR.

3.7. Degradation

A controlled degradation of the hydrogels in two different environments was performed. Fig. 9A shows the results of the enzymatic degradation for the hydrogels ranging from 8.6 % to 18.9 % during the first 24 h, and from 6.6 % to 21.2 % for 48 h.

The first conclusion is that extending the experiment from 24 h to 48 h did not significantly increase the degradation rate of the hydrogels, suggesting that most of the degradation occurred within the initial hours of exposure to the fluid. The hydrogels containing astaxanthin showed higher degradation in PECF + lyz compared to hydrogel B which could be due to the preferential binding of astaxanthin to lysozyme mainly through hydrophobic interactions [68]. In contrast, the hydrogels containing ozonized oils, BOz8_2 and BOz12_2, showed significantly lower degradation in PECF + lyz than hydrogel B at both 24 h and 48 h. According to the literature, ozone inhibits the enzymatic activity of lysozyme [69], which could have contributed to the reduced degradation that remained under 10 % in both samples for the two time periods. The slight tendency for higher degradation at 24 h than at 48 h (1–3 % variation) might be explained by a swelling event surpassing the low degradation, therefore culminating in an increase in hydrogel mass even after spending an extra 24 h immersed in the degradation solution. This effect has also been reported by Ekasurya et al. [70].

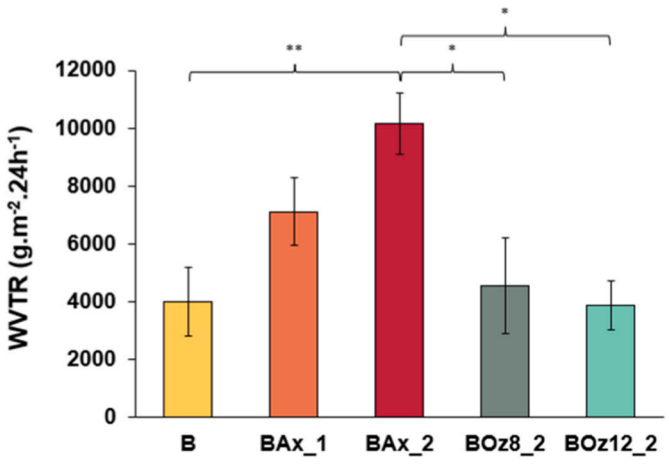

Fig. 8. WVTR results of the hydrogels. The error bars represent the ±mean standard deviations (n = 3).

Regarding the hydrolytic degradation conducted in PBS (Fig. 9B), the weight loss of these hydrogels ranged from 0.1 % to 8.6 % during the first 24 h, and from 1.9 % to 13.1 % for 48 h. In this case, the longer the hydrogel remained immersed in the degradation solution, the greater the weight loss observed. The hydrogels containing astaxanthin suffered the highest average degradation, while the hydrogels with incorporated ozonized oils presented minor weight losses. Hydrogel BOz8_2 exhibited a peculiar behavior with vestigial weight loss in the first 24 h. While it might seem that the hydrogel did not degrade after one day in PBS, a more likely explanation is that swelling offset any degradation, balancing the overall weight change.

Comparison of the weight losses obtained from both tests shows that enzymatic solution promoted higher degradation for all hydrogels. Hydrogel B exhibited moderate degradation. BAx_1 and BAx_2 hydrogels experienced the highest levels of degradation, while BOz8_2 and BOz12_2, showed the least weight loss. This suggests that astaxanthin may promote higher degradation rates, while ozonized oils seem to play a protective role in hydrogel degradation, including in the presence of enzymatic agents. The different influence of astaxanthin and ozonized oils on the material's resistance to degradation may be attributed to the observed changes in the hydrogel structure (Fig. 4): while astaxanthin increased the porosity of the hydrogels, ozonized oils had only a slight effect.

3.8. Tensile behavior

The mechanical properties of the hydrogels were initially evaluated using tensile tests. Representative curves for each hydrogel formulation are presented in Fig. 10A, which show that, as expected, all hydrogels exhibited an elastomer-like behavior. The values of Young's modulus for each hydrogel are depicted in Fig. 10B.

Hydrogels B and BOz8_2 are the stiffest hydrogels, indicating better structural support, which may be beneficial for wounds located in body areas subjected to the patient movement. In the case of BAx_2, the modulus of elasticity decreased more than 50 % (27.5 ± 3.0 kPa) compared to hydrogel B ($p = 0.0001$). The mechanical properties of this hydrogel are likely to be due to interactions between astaxanthin and the hydrogel matrix, which affect the crosslinking structure, elasticity, and stretchability of the material. The differences between the mechanical properties of BAx_2 and BAx_1 reflect the different amounts of astaxanthin present in the hydrogel.

In comparison with astaxanthin, the incorporation of ozonized oils had a small effect on the mechanical properties of the hydrogels. The modulus of elasticity of hydrogel BOz8_2 is similar to that of hydrogel B ($p = 0.7034$), while hydrogel BOz12_2 exhibited a Young's modulus value ~20 % lower than hydrogel B ($p = 0.0179$), revealing some detrimental effects on the mechanical properties.

The values of the Young's modulus of our hydrogels (27.5–59.1 kPa) lie near the lower limit of the range reported by Minsart et al. [71] for commercial wound dressings (50 kPa), and within the range of values described by Massarelli et al. [11] for PVA/chitosan wound dressings. Similarly, Drury et al. [72] and Peng et al. [73] registered Young's moduli of alginate hydrogels and PVA/chitosan hydrogels in the same range. It is important to stress that dressings with high Young's modulus may limit body movement causing trauma, while low Young's modulus dressings are difficult to keep on the wound surface.

The ultimate tensile stress is presented in Fig. 10C. Hydrogel B exhibited the highest tensile strength (66.2 ± 3.6 kPa), while the incorporation of astaxanthin, particularly at higher concentrations (BAx_2), led to a significant reduction in strength (28.2 ± 9.4 kPa, $p = 0.0002$). This observation is consistent with the previously discussed

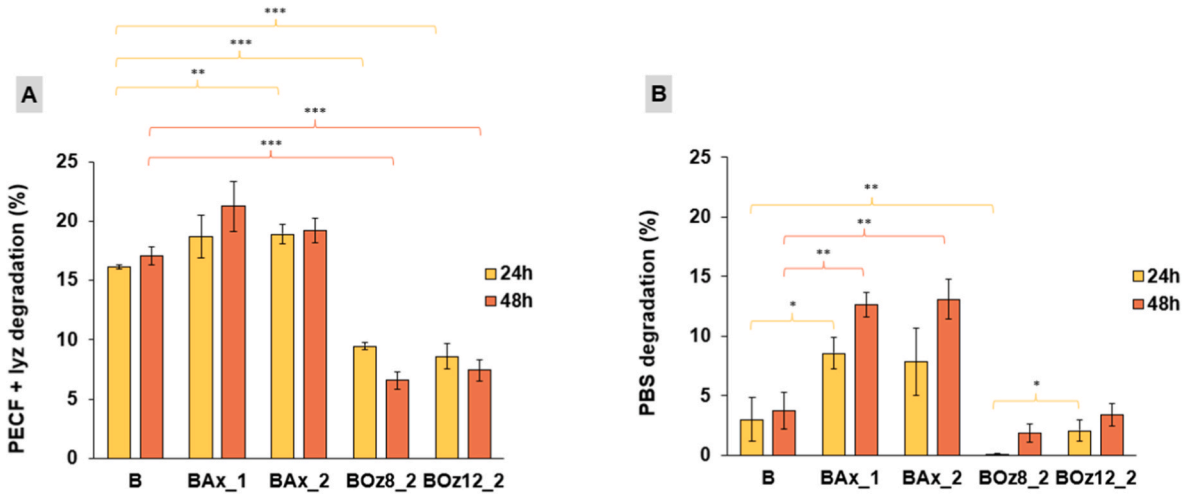

Fig. 9. Degradation of the hydrogels after 24 h and 48 h in (A) PECF + lyz and (B) PBS. The error bars represent the ±mean standard deviations (n = 3).

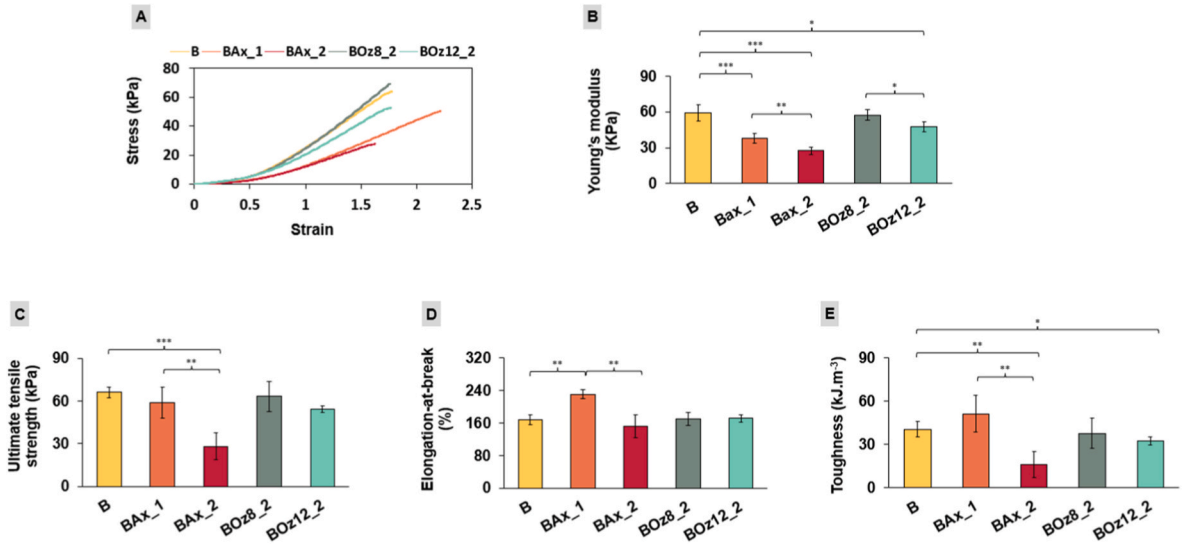

Fig. 10. (A) Tensile stress-strain curves, (B) Young's modulus, (C) ultimate tensile strength, (D) elongation-at-break and (E) toughness of the hydrogels.

decrease in stiffness for BAx_2 and suggests that astaxanthin interferes with the polymeric network, weakening intermolecular interactions and limiting stress transfer across the hydrogel matrix. In contrast, hydrogels containing ozonized oils (BOz8_2 and BOz12_2) retained mechanical strength values similar to or slightly lower than the control hydrogel B, indicating a less pronounced effect of these bioactive agents on tensile resistance.

The elongation-at-break (Fig. 10 D) highlights another important aspect of the hydrogel's mechanical behavior. Interestingly, hydrogel BAx_1 showed the highest value (230.9 ± 11.1 %), significantly higher than hydrogel B ($p = 0.0056$). This suggests that a lower concentration of astaxanthin may slightly alter the hydrogel network, for instance by modulating polymer–polymer interactions and allowing greater chain mobility, which results in an increased strain at break. By contrast, BAx_2 displayed elongation values similar to the control hydrogel B ($p = 0.316$), but significantly lower than BAx_1 ($p = 0.0094$). This indicates that the effect observed at lower astaxanthin concentration does not persist at higher levels, where the balance between polymer–polymer and polymer–astaxanthin interactions may counteract the increase in the strain capacity. Hydrogels with ozonized oils (BOz8_2 and BOz12_2) presented elongation values comparable to hydrogel B, suggesting that these bioactive agents do not alter the strain capacity of the hydrogel matrix.

The toughness values of the hydrogels are shown in Fig. 10E. The incorporation of astaxanthin induced a concentration-dependent trend: BAx_1 presented a slight increase compared to the control, although this difference was not statistically significant ($p = 0.104$), suggesting that low concentrations of astaxanthin may promote minor reinforcement or plasticization effects without substantially altering the structural integrity of the network. In contrast, BAx_2 showed a significant reduction ($p = 0.0025$), evidencing that higher astaxanthin content compromises the hydrogel's capacity to dissipate energy, likely due to perturbations in polymer–polymer interactions and reduced synergy in the crosslinked structure. For hydrogels with ozonized oils, the effect on toughness was more limited. BOz8_2 maintained values similar to hydrogel B ($p = 0.639$), while BOz12_2 exhibited only a slight but significant reduction ($p = 0.029$). The toughness values reported (16–51 kJ m^{-3}) are within the range of hydrogels designed for wound dressing applications, as observed in previous works [74,75].

3.9. Rheological behavior

The evaluation of the viscoelasticity of the hydrogels was carried out through rheological testing. The changes in the storage (G′) and loss (G″)

moduli, respectively associated with elastic and viscous behavior, versus the angular frequency are shown in Fig. 11.

All hydrogels presented a predominant elastic response for all frequencies since G′ (ω) > G″ (ω), a characteristic of viscoelastic materials. The storage modulus (G′) remained nearly constant throughout the frequency range for all hydrogels. Conversely, the loss modulus (G″) demonstrated a wavy pattern for some hydrogels, namely in the case of BAx_2.

The incorporation of astaxanthin in the hydrogel matrix led to a decrease in both moduli comparing to hydrogel B. This, together with the observed variations of the moduli with frequency suggests the presence of heterogeneities in the hydrogel structure that are responsible for detrimental rheological properties of astaxanthin-containing hydrogels.

Concerning the hydrogels with ozonized oils, BOz12_2 presented values for both moduli similar to those of hydrogel B, while BOz8_2 exhibited G′ and G″ values lower than hydrogel B. This means that the degree of ozonation of the oil affected the viscoelastic behavior of the hydrogel: a lower degree led to a more deformable material with lower damping response.

The loss tangent (tan δ) defined as the ratio between the loss and the storage moduli allowed the determination of the phase angle (δ), which gives a relative measure of the viscous and elastic characteristics of the material. For instance, δ of 90° indicates a purely viscous material, while for a pure elastic material δ would be equal to 0° [76]. Table 2 shows the results obtained for the phase angle of the hydrogels tested, which ranged from (3.0 ± 1.2) ° to (5.1 ± 2.2) °.

This range of values means that all hydrogels displayed properties close to elastic-like materials. Addition of active agents in the formulations of the hydrogels slightly enhanced their elasticity since hydrogel B presented the highest phase angle (δ).

Comparison with other studies reveals that the viscoelastic behavior of our hydrogels, characterized by G' (450–1900 Pa) and G'' (4–150 Pa), is comparable to other PVA hydrogels proposed for wound dressings. Soto-Bustamante et al. [77] produced PVA/chitosan hydrogels varying both the composition and the FT time and obtained storage and loss moduli values of the same order of magnitude of those found in the of the present work. For example, the composition PVA/chitosan 70/30 led to G' (500–900 Pa) and G'' (40–100 Pa), depending on the number of FT cycles. Rainho et al. [78] reported the storage moduli obtained in the range of 10^2–10^3 Pa and the loss moduli ranging between 1 and 10^3 Pa for PVA/casein hydrogels. Overall, the values obtained for G′ and G″ regarding the hydrogels developed in this work fall within the optimal range for wound dressing materials, especially for hydrogel-based or soft elastomeric dressings. In fact, they suggest that the materials shall be soft enough to be gentle and conformable to skin/tissue, but simultaneously structurally sound enough to maintain integrity. Besides, they shall present a balanced viscoelasticity suitable for moisture retention and wound protection.

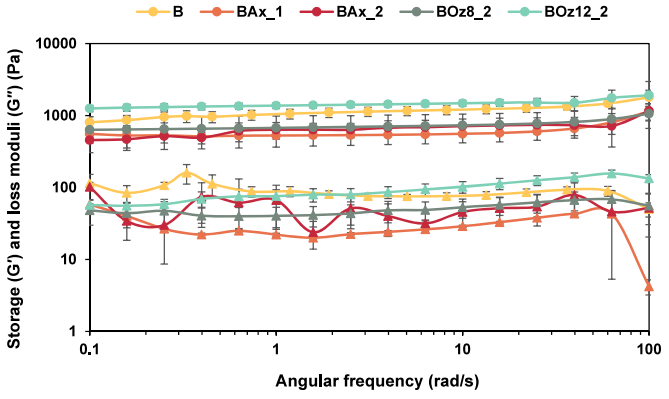

Fig. 11. Storage (G′) (circle symbols) and loss (G″) (triangle symbols) moduli of the hydrogels obtained by rheological measurements. The error bars represent the ±mean standard deviations (n = 3).

Table 2
Phase angles (δ) obtained by the loss factor (tan δ). The error bars represent the ±mean standard deviations (n = 3).

Hydrogel	δ (°)
B	5.1 ± 2.2
BAx_1	3.0 ± 1.2
BAx_2	4.7 ± 2.4
BOz8_2	4.2 ± 0.7
BOz12_2	3.7 ± 1.0

3.10. Mucoadhesion

The mucoadhesion tests were performed to predict the adhesiveness of the hydrogels to the wound bed. Fig. 12 A and B show the maximum force of detachment and the work of adhesion, respectively.

Hydrogel B was the least adhesive with maximum force of detachment of 85.1 mN and work of adhesion of 68.7 mN mm. These values suggested that hydrogel B should be suitable for some applications where low adhesion is preferred. BAx_1 was the hydrogel with both strongest force and highest work of adhesion (188.9 mN and 904.8 mN mm, respectively), which indicates that this hydrogel exhibits the greatest ability to adhere to a skin-like surface and shows a high resistance to detachment. The hydrogel BOz12_2 presented the second highest values for the maximum force (187.2 mN) and work of adhesion (618.1 mN mm). Despite the difficulty to directly correlate the mucoadhesive properties with the type and amount of active agents, the results show that the presence of these agents enhance the adhesiveness of the hydrogels, which may be related to the structural characteristics of the hydrogels and eventual interactions between the agent molecules and the mucosal surface.

Optimization of the adherence of the dressing to the wound is a complex issue. Good adherence not only promotes tissue bonding but also conforms to the topography of the wound bed, which can help reduce pain [79]. In contrast, other authors call attention to the fact that adhesion of the dressing to the wound surface should be minimized to prevent trauma of the vulnerable skin during the removal process [80]. Thus, the ideal adhesive should be selected taking into consideration several factors, such as the type of wound, patient characteristics, and environment [81].

3.11. Biological activity

Fig. 13A displays the CAMs after being in contact with the hydrogel discs for 5 min. Throughout the test, no signs of coagulation, hemorrhage, or vascular lysis were observed in any of the CAMs. Therefore, all hydrogels obtained an irritation score of 0.0 % and may be classified as non-irritating materials.

The hemocompatibility results, given in Fig. 13B, show how the hydrogels interact with red blood cells. The hemolysis ratio varied from 0.2 % to 1.2 %, indicating minimal impact on the cells. According to ASTM F756-00 [36], materials can be classified based on their hemolysis ratio: above 5 % are deemed hemolytic, between 2 % and 5 % are considered slightly hemolytic, and below 2 % are categorized as non-hemolytic. Thus, all hydrogels are highly compatible with red blood cells since they led to hemolysis ratios below 2 %.

Fig. 13C presents the cytotoxicity results. The hydrogels may be considered non-toxic since cell viability was not significantly different from the negative control, demonstrating values above those defined by the ISO 10993-5 standard [37]. The quantity of astaxanthin in the hydrogel formulation had a clear positive impact on the viability of the fibroblasts, as BAx_2 led to an increase of 25.3 % comparatively to BAx_1

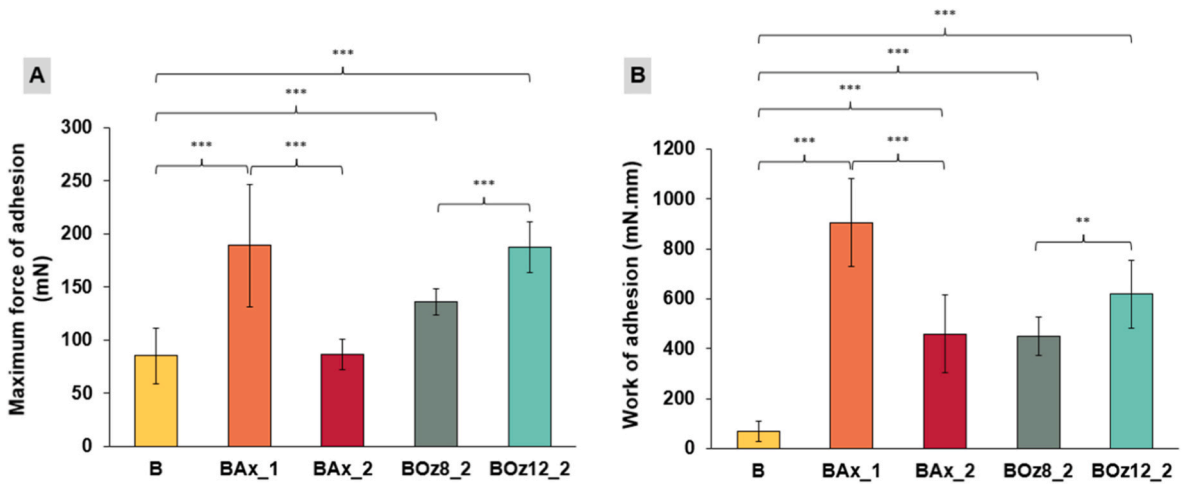

Fig. 12. (A) Maximum detachment forces and (B) work of adhesion of the hydrogels determined by the mucoadhesion tests. The error bars represent the ±mean standard deviations (n = 3).

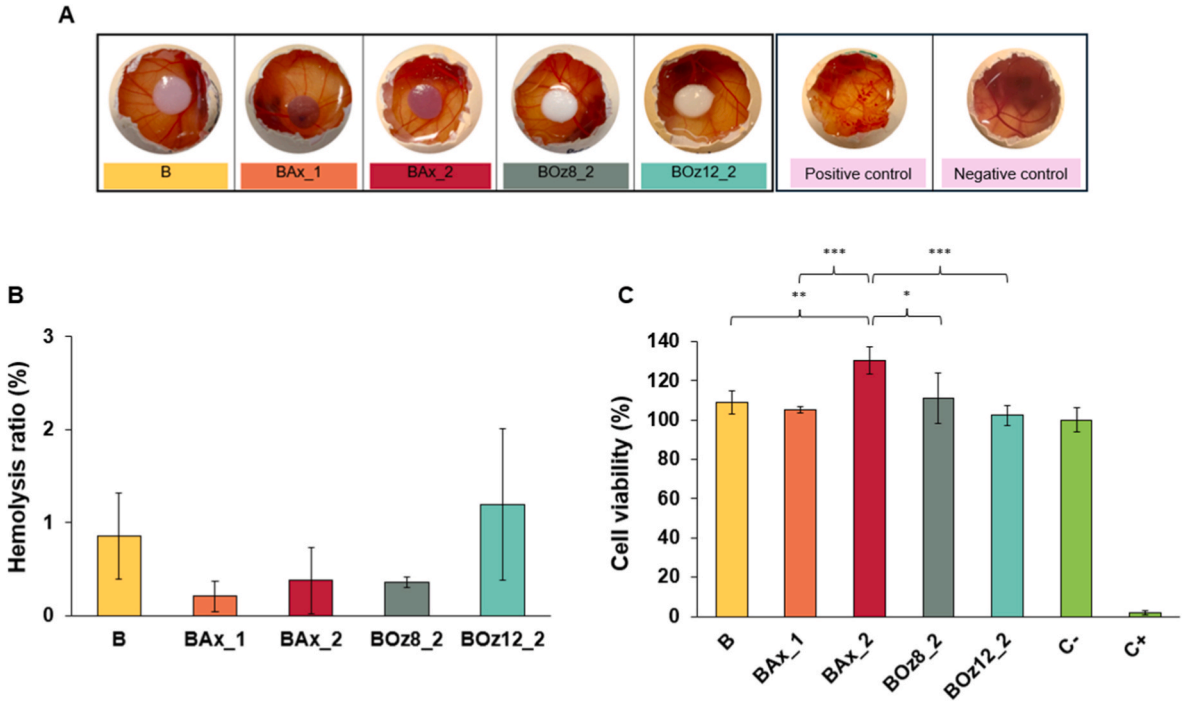

Fig. 13. (A) CAM images after 5 min in contact with hydrogel discs. Negative and positive controls are also shown. (B) Hemolysis ratio (%); (C) Cell viability of fibroblasts after exposure to extracts of hydrogels for 24 h. The error bars represent ± standard deviations.

($p = 0.0004$). On the other hand, the type of ozonized oil had a small influence since the difference between BOz8_2 and BOz12_2 ($p = 0.2662$) is only 8.5 %.

The capacity of the hydrogel formulations to inhibiting bacterial growth was tested against several strains of Gram-positive and Gram-negative bacteria, *Enterococcus faecium* and *Escherichia coli* respectively. Overall, the discs did not prevent the growth of vancomycin susceptible *E. faecium, E. coli* and ESBL strains. However, the growth of three strains of VRE (VRE1, VRE2 and VRE4) was inhibited by some hydrogels. Table 3 shows the dimensions of the inhibition halos for the different hydrogels and strains.

All hydrogels presented some antibacterial capacity, even hydrogel B without active agents in its formulation. The result of the latter hydrogel could be related to the presence of casein and chitosan in its composition, which, as previously mentioned, are known for their antimicrobial properties. The inherent positive charge of chitosan and casein at low pH enables the attachment of the negatively charged bacterial membranes. Several authors have reported the antimicrobial activity of these compounds, namely Flores-Nieves et al. [82], who found that electrospun

Table 3
Dimensions of inhibition halos (mm) in antimicrobial susceptibility tests performed with the hydrogels against different VRE strains.

Bacteria strain	Diameter of inhibition halo (mm)				
	B	BAx_1	BAx_2	BOz8_2	BOz12_2
VRE1	6	7	7	6	6
VRE2	–	6	–	–	8
VRE4	–	–	–	–	8

casein fibers had inhibitory effect against *E. coli* bacteria, and Aziz et al. [83], who produced a chitosan/dextran-based hydrogel effective against the same bacteria.

The growth of both ESBL and non-ESBL-producing strains of *E. coli* was not inhibited by the presence of the hydrogels. This lack of inhibition could be associated with the composition of the cell walls of the Gram-negative bacteria. These bacteria have a cell envelope, which comprises an outer membrane, the thinner peptidoglycan cell wall, and finally an inner membrane. The outer membrane consists of a lipid bilayer composed of glycolipids with lipid tails of hydrophobic nature [84]. Gram-negative bacteria can change the hydrophobic properties or mutations in this outer membrane, consequently increasing their resistance to antibiotics [85].

Among the Gram-positive strains, only some VRE were inhibited, while the non-VRE grew as much as the *E. coli*. VRE1 was the unique strain that was inhibited by all hydrogels. The blockage to growth of this strain was independent of the type of active agent present in the hydrogel. BOz12_2 stood up as the hydrogel with the highest antimicrobial activity, inhibiting the growth of three bacterial strains. These results agree with the findings of Song et al. [86], who studied the antibacterial effects of ozonized oil and ozonized water against *S. aureus* and methicillin resistant *S. aureus* (MRSA) for topical applications in skin infections. They reported that the ozonized oil had powerful antibacterial properties, particularly against Gram-positive microorganisms.

The ability of BOz12_2 to inhibit multiple strains of multidrug-resistant *Enterococcus* is particularly relevant in the context of diabetic foot ulcers, where these pathogens are often implicated and therapeutic options are increasingly limited. In contrast, the absence of inhibition against *E. coli* strains, both ESBL and non-ESBL, likely reflects the barrier function of the Gram-negative outer membrane, which limits the penetration of both hydrophilic and lipophilic agents. This structural feature, combined with potential efflux mechanisms, can reduce the efficacy of topically applied antimicrobial formulations.

It is also important to consider the limitations of the disc diffusion method employed in this study. The method relies on radial diffusion of antimicrobial agents through an agar matrix, which may underestimate the bioactivity of hydrophobic compounds such as astaxanthin and ozonized oils. Their low water solubility and restricted diffusion radius can result in small or absent inhibition zones, even when bactericidal effects are present at the site of contact. In the future, other methods based on direct contact in suspension will be used to better assess the antimicrobial activity.

4. Conclusions

The main objective of this work was to develop hydrogels with enhanced properties to accelerate the healing of chronic wounds. The focus was on PVA/casein/chitosan-based hydrogels, integrating two active agents – astaxanthin and ozonized oils. Astaxanthin was selected due to its antioxidant properties, while the choice of ozonized oils was based on their reported antimicrobial, anti-inflammatory, and wound debridement properties. The hydrogels were produced using the FT method that induces the formation of a porous structure. This porosity is advantageous for wound dressings, impacting water absorption, mechanical properties, and potentially enhancing drug delivery.

The hydrogels were initially evaluated for their antioxidant capacity, given the critical role of oxidative balance in wound healing. Incorporation of astaxanthin and ozonized oils significantly enhanced their free-radical–scavenging activity, a key requirement for managing diabetic wounds. Four hydrogels were selected for further characterization, namely BAx_1 and BAx_2 with varying concentrations of astaxanthin; and BOz12_2 and BOz8_2 with differences in ozonation degree and oil composition. Water content of the hydrogels increased with the addition of the active agents; meanwhile swelling capacity decreased. All hydrogels, except BAx_2, presented adequate WVTR values. The degradation studies showed that hydrogels experienced higher enzymatic degradation than hydrolytic, and it was more significative for blank and astaxanthin loaded hydrogels. Both ozonized oils and astaxanthin led to the weakening of the mechanical properties of the hydrogels and increased their mucoadhesiveness.

In terms of the biological activity, none of the hydrogels were cytotoxic nor irritant, and all presented good compatibility with blood. The hydrogels, including B without active agents, exhibited some antibacterial capacity attributed to casein and chitosan. Notably, BOz12_2 demonstrated the highest antimicrobial activity, inhibiting the growth of three bacterial strains, particularly the VRE. The study also highlights the need for complementary antimicrobial assays to more accurately assess the efficacy of hydrophobic actives in hydrogel matrices.

Overall, it is possible to conclude that the studied formulations enabled the production of hydrogels with promising properties for wound dressing applications. The hydrogel BOz12_2 was the material that gathered the best therapeutic properties, namely high antioxidant activity and wide antibacterial effects.

Future research should focus on applications where a targeted delivery of drugs is required to maximize the therapeutic benefits of the dressings and improve patient outcomes. Furthermore, clinical trials are necessary to validate the efficacy and safety of these innovative wound care solutions in a real-world setting.

CRediT authorship contribution statement

M. Gonçalves: Validation, Investigation, Formal analysis, Data curation. **A.C. Branco:** Writing – original draft, Data curation. **V. Silva:** Investigation, Data curation. **D.C. Silva:** Writing – review & editing, Methodology. **M. Salema-Oom:** Writing – review & editing, Resources, Methodology, Investigation, Formal analysis, Data curation. **J. Coelho:** Methodology. **R. Colaço:** Resources, Funding acquisition. **R. Galante:** Writing – review & editing, Supervision, Project administration, Methodology, Funding acquisition, Conceptualization. **P. Poeta:** Methodology, Funding acquisition. **B. Saramago:** Writing – original draft. **A.P. Serro:** Writing – review & editing, Supervision, Resources, Project administration, Methodology, Conceptualization.

Declaration of competing interest

The authors declare that they have no known competing financial interests or personal relationships that could have appeared to influence the work reported in this paper.

Acknowledgements

To FCT for funding through projects https://doi.org/10.54499/UIDB/00100/2020 and https://doi.org/10.54499/UIDP/00100/2020 (CQE), https://doi.org/10.54499/UIDB/50022/2020 (LAETA), and https://doi.org/10.54499/2022.03408.PTDC (Milk4WoundCare). Diana C. Silva acknowledges FCT for her Junior Research contract https://doi.org/10.54499/2022.08560.CEECIND/CP1713/CT0016. Acknowledgements are also due to Eng. Paula Matos from Laboratório de Radioesterilização (C2TN-IST) for the gamma irradiation of material used in cytotoxicity tests.

Appendix A. Supplementary data

Supplementary data to this article can be found online at https://doi.org/10.1016/j.mtchem.2025.103059.

Data availability

Data will be made available on request.

References

[1] U. Galicia-Garcia, A. Benito-Vicente, S. Jebari, A. Larrea-Sebal, H. Siddiqi, K. B. Uribe, H. Ostolaza, C. Martín, Pathophysiology of type 2 diabetes mellitus, Int. J. Mol. Sci. 21 (2020) 1–34, https://doi.org/10.3390/ijms21176275.

[2] IDF Diabetes Atlas https://Diabetesatlas.Org/.

[3] Lifestyles matter in the prevention of type 2 diabetes. http://diabetesjournals.org/care/article-pdf/25/9/1650/590171/dc0902001650.pdf.

[4] S.F. Spampinato, G.I. Caruso, R. De Pasquale, M.A. Sortino, S. Merlo, The treatment of impaired wound healing in diabetes: looking among old drugs, Pharmaceuticals 13 (2020) 60, https://doi.org/10.3390/ph13040060.

[5] M. Mieczkowski, B. Mrozikiewicz-Rakowska, M. Kowara, M. Kleibert, L. Czupryniak, The problem of wound healing in diabetes—from molecular pathways to the design of an animal model, Int. J. Mol. Sci. 23 (2022) 7930, https://doi.org/10.3390/ijms23147930.

[6] Q. Yang, D. Fang, J. Chen, S. Hu, N. Chen, J. Jiang, M. Zeng, M. Luo, LncRNAs associated with oxidative stress in diabetic wound healing: regulatory mechanisms and application prospects, Theranostics 13 (2023) 3655–3674, https://doi.org/10.7150/thno.85823.

[7] J.L. Burgess, W.A. Wyant, B.A. Abujamra, R.S. Kirsner, I. Jozic, Diabetic wound-healing science, Medicina (Lithuania) 57 (2021) 1072, https://doi.org/10.3390/medicina57101072.

[8] W. Zhang, L. Chen, Y. Xiong, A.C. Panayi, A. Abududilibaier, Y. Hu, C. Yu, W. Zhou, Y. Sun, M. Liu, H. Xue, L. Hu, C. Yan, X. Xie, Z. Lin, F. Cao, B. Mi, G. Liu, Antioxidant therapy and antioxidant-related bionanomaterials in diabetic wound healing, Front. Bioeng. Biotechnol. 9 (2021) 707479, https://doi.org/10.3389/fbioe.2021.707479.

[9] S. Tavakoli, A.S. Klar, Advanced hydrogels as wound dressings, Biomolecules 10 (2020) 1–20, https://doi.org/10.3390/biom10081169.

[10] H. Chopra, S. Bibi, S. Kumar, M.S. Khan, P. Kumar, I. Singh, Preparation and evaluation of Chitosan/PVA based hydrogel films loaded with honey for wound healing application, Gels 8 (2022) 111, https://doi.org/10.3390/gels8020111.

[11] E. Massarelli, D. Silva, A.F.R. Pimenta, A.I. Fernandes, J.L.G. Mata, H. Armês, M. Salema-Oom, B. Saramago, A.P. Serro, Polyvinyl alcohol/chitosan wound dressings loaded with antiseptics, Int. J. Pharm. 593 (2021) 120110, https://doi.org/10.1016/j.ijpharm.2020.120110.

[12] J. Fu, F. Yang, Z. Guo, The chitosan hydrogels: from structure to function, New J. Chem. 42 (2018) 17162–17180, https://doi.org/10.1039/C8NJ03482F.

[13] S.G. Jin, Production and application of biomaterials based on polyvinyl alcohol (PVA) as wound dressing, Chem. Asian J. 17 (2022) e202200595, https://doi.org/10.1002/asia.202200595.

[14] S. Abbasinia, R. Monfared-Hajishirkiaee, H. Ehtesabi, Nanocomposite sponge based on sodium alginate, polyvinyl alcohol, carbon dots, and woolly hedge nettle antibacterial extract for wound healing, Ind. Crops Prod. 214 (2024) 118554, https://doi.org/10.1016/j.indcrop.2024.118554.

[15] M. Ziyazadeh, M. Vafaiee, R. Mohammadpour, H. Ehtesabi, Dual-sided and flexible triboelectric nanogenerator-based hydrogel skin patch for promoting wound healing, Nano Energy 134 (2025) 110558, https://doi.org/10.1016/j.nanoen.2024.110558.

[16] M.A. Matica, F.L. Aachmann, A. Tøndervik, H. Sletta, V. Ostafe, Chitosan as a wound dressing starting material: antimicrobial properties and mode of action, Int. J. Mol. Sci. 20 (2019) 5889, https://doi.org/10.3390/ijms20235889.

[17] C.L. Ke, F.S. Deng, C.Y. Chuang, C.H. Lin, Antimicrobial actions and applications of Chitosan, Polymers 13 (2021) 904, https://doi.org/10.3390/polym13060904.

[18] S.J. Jeon, M. Oh, W.S. Yeo, K.N. Galvão, K.C. Jeong, Underlying mechanism of antimicrobial activity of chitosan microparticles and implications for the treatment of infectious diseases, PLoS One 9 (2014) e92723, https://doi.org/10.1371/journal.pone.0092723.

[19] S. Rajinikanth B, D.S.R. Rajkumar, K. K, V. Vijayaragavan, Chitosan-based biomaterial in wound healing: a review, Cureus (2024) e55193, https://doi.org/10.7759/cureus.55193.

[20] X. Zhang, M. Qin, J. Jia, A. Ahmed, L. Zhao, W. Lan, Y. Wei, Z. Liang, X. Ma, Y. Shi, D. Huang, A natural gelatin/casein hydrogel with on-demand adhesion via chitosan solution for wound healing, Int. J. Biol. Macromol. 290 (2025) 139112, https://doi.org/10.1016/j.ijbiomac.2024.139112.

[21] L.V. Garcia, D. Silva, M.M. Costa, H. Armés, M. Salema-Oom, B. Saramago, A. P. Serro, Antiseptic-loaded casein hydrogels for wound dressings, Pharmaceutics 15 (2023) 334, https://doi.org/10.3390/pharmaceutics15020334.

[22] L. Deng, C. Du, P. Song, T. Chen, S. Rui, D.G. Armstrong, W. Deng, The role of oxidative stress and antioxidants in diabetic wound healing, Oxid. Med. Cell. Longev. 2021 (2021) 8852759, https://doi.org/10.1155/2021/8852759.

[23] X. Zhao, Y.J. Cui, S.S. Bai, Z.J. Yang, Miao-Cai, S. Megrous, T. Aziz, A. Sarwar, D. Li, Z.N. Yang, Antioxidant activity of novel casein-derived peptides with microbial proteases as characterized via Keap1-Nrf2 pathway in HepG2 cells, J. Microbiol. Biotechnol. 31 (2021) 1163–1174, https://doi.org/10.4014/jmb.2104.04013.

[24] R.K. Thapa, K.G. Grønlien, H.H. Tønnesen, Protein-based systems for topical antibacterial therapy, Front Med Technol 3 (2021) 685686, https://doi.org/10.3389/fmedt.2021.685686.

[25] M. Stobiecka, J. Król, A. Brodziak, Antioxidant activity of milk and dairy products, Animals 12 (2022) 245, https://doi.org/10.3390/ani12030245.

[26] K.H. Cho, J.E. Kim, A. Bahuguna, D.J. Kang, Ozonated sunflower oil exerted potent anti-inflammatory activities with enhanced wound healing and tissue regeneration abilities against acute toxicity of carboxymethyllysine in zebrafish with improved blood lipid profile, Antioxidants 12 (2023) 1625, https://doi.org/10.3390/antiox12081625.

[27] V. Silva, C. Peirone, J.S. Amaral, R. Capita, C. Alonso-Calleja, J.A. Marques-Magallanes, Á. Martins, Á. Carvalho, L. Maltez, J.E. Pereira, J.L. Capelo, G. Igrejas, P. Poeta, High efficacy of ozonated oils on the removal of biofilms produced by methicillin-resistant Staphylococcus aureus (MRSA) from infected diabetic foot ulcers, Molecules 25 (2020) 3601, https://doi.org/10.3390/molecules25163601.

[28] V. Silva, C. Peirone, R. Capita, C. Alonso-Calleja, J.A. Marques-Magallanes, I. Pires, L. Maltez, J.E. Pereira, G. Igrejas, P. Poeta, Topical application of ozonated oils for the treatment of MRSA skin infection in an animal model of infected ulcer, Biology 10 (2021) 372, https://doi.org/10.3390/biology10050372.

[29] J. Meephansan, A. Rungjang, W. Yingmema, R. Deenonpoe, S. Ponnikorn, Effect of astaxanthin on cutaneous wound healing, Clin. Cosmet. Invest. Dermatol. 10 (2017) 259–265, https://doi.org/10.2147/CCID.S142795.

[30] S. Davinelli, M.E. Nielsen, G. Scapagnini, Astaxanthin in skin health, repair, and disease: a comprehensive review, Nutrients 10 (2018) 552, https://doi.org/10.3390/nu10040522.

[31] M.X. Chang, F. Xiong, Astaxanthin and its effects in inflammatory responses and inflammation-associated diseases: recent advances and future directions, Molecules 25 (2020) 5342, https://doi.org/10.3390/MOLECULES25225342.

[32] S.B. Kedare, R.P. Singh, Genesis and development of DPPH method of antioxidant assay, J. Food Sci. Technol. 48 (2011) 412–422, https://doi.org/10.1007/s13197-011-0251-1.

[33] Standard Test Methods for Water Vapor Transmission of Materials, ASTM, 1995. E96-95.

[34] ICCVAM, The hen's egg test –Chorioallantoic membrane test method, in: ICCVAM Test Method Evaluation Report: Current Validation Status of in Vitro Test Methods Proposed for Identifying Eye Injury Hazard Potential of Chemicals and Products, NIH Publication No. 10-7553. National Institute of Environmental Health Sciences, North Carolina, Research Triangle Park, 2010, pp. 19–25.

[35] P. Rainho, M. Salema-Oom, C.A. Pinto, J.A. Saraiva, B. Saramago, D.C. Silva, A. P. Serro, Polyvinyl alcohol/casein hydrogels with oxymatrine eluting ability for cancer-related wound management, Biomater. Sci. 13 (2025) 2755–2766, https://doi.org/10.1039/D5BM00191A.

[36] Practice for assessment of hemolytic properties of materials. https://doi.org/10.1520/F0756-17, 2017.

[37] International Organization for Standardization, ISO 10993-5 Biological Evaluation of Medical Devices - Part 5: Tests for in Vitro Cytotoxicity, 2009.

[38] M. Anraku, J.M. Gebicki, D. Iohara, H. Tomida, K. Uekama, T. Maruyama, F. Hirayama, M. Otagiri, Antioxidant activities of chitosans and its derivatives in in vitro and in vivo studies, Carbohydr. Polym. 199 (2018) 141–149, https://doi.org/10.1016/j.carbpol.2018.07.016.

[39] T.H.P. Brotosudarmo, L. Limantara, E. Setiyono, Heriyanto, structures of astaxanthin and their consequences for therapeutic application, Int J Food Sci 2020 (2020) 215658, https://doi.org/10.1155/2020/2156582.

[40] M. Dai, C. Li, Z. Yang, Z. Sui, J. Li, P. Dong, X. Liang, The astaxanthin aggregation pattern greatly influences its antioxidant activity: a comparative study in CACO-2 cells, Antioxidants 9 (2020) 126, https://doi.org/10.3390/antiox9020126.

[41] K.H. Cho, D.J. Kang, H.S. Nam, J.H. Kim, S.Y. Kim, J.O. Lee, B.J. Kim, Ozonated sunflower oil exerted protective effect for embryo and cell survival via potent reduction power and antioxidant activity in HDL with strong antimicrobial activity, Antioxidants 10 (2021) 1651, https://doi.org/10.3390/antiox10111651.

[42] M. Gorzynik-Debicka, P. Przychodzen, F. Cappello, A. Kuban-Jankowska, A. M. Gammazza, N. Knap, M. Wozniak, M. Gorska-Ponikowska, Potential health benefits of olive oil and plant polyphenols, Int. J. Mol. Sci. 19 (2018) 686, https://doi.org/10.3390/ijms19030686.

[43] F.J. Sánchez-Muniz, C. Cuesta, Sunflower oil, in: Encyclopedia of Food Sciences and Nutrition, Elsevier, 2003, pp. 5672–5680, https://doi.org/10.1016/B0-12-227055-X/01351-1.

[44] P.R. Sonar, A.S. Panchbhai, A.G. Ghom, S. Dole, Comparative evaluation of efficacy of topical ozonated olive oil and topical chlorhexidine gluconate in management of recurrent aphthous stomatitis, International Arab Journal of Dentistry 15 (2024) 29–37, https://doi.org/10.70174/iajd.v15i1.955.

[45] H.E. Snyder, L.A. Wilson, Soy (Soya) beans | processing for the food industry, in: Encyclopedia of Food Sciences and Nutrition, Elsevier, 2003, pp. 5383–5389, https://doi.org/10.1016/B0-12-227055-X/01110-X.

[46] A. Türk Baydir, A. Türk Baydır, Ç. Aşçıoğlu, A.K. Üniversitesi, Effects of antioxidant capacity and peroxide value on oxidation stability of sunflower oil, Chem. Mater. 1 (2018) 5–7. https://www.researchgate.net/publication/346421114.

[47] N.R. Almeida, A. Beatriz, A.C. Micheletti, E.J. de Arruda, Ozonized vegetable oils and therapeutic properties: a review, Orbital - Electron. J. Chem. 4 (2013) 313–326, https://doi.org/10.17807/orbital.v4i4.467.

[48] A.S. Oliveira, O. Seidi, N. Ribeiro, R. Colaço, A.P. Serro, Tribomechanical comparison between PVA hydrogels obtained using different processing conditions and human cartilage, Materials 12 (2019) 3413, https://doi.org/10.3390/ma12203413.

[49] K. Kawanishi, M. Komatsu, T. Inouet, Thermodynamic consideration of the sol-gel transition in polymer solutions, Polymer 28 (1987) 980–984, https://doi.org/10.1016/0032-3861(87)90173-X.

[50] P. Da Hong, C.M. Chou, W.T. Chuang, Effects of mixed solvent on gelation of poly (vinyl alcohol) solutions, J. Appl. Polym. Sci. 79 (2001) 1113–1120, https://doi.org/10.1002/1097-4628(20010207)79:6<1113::AID-APP150>3.0.CO;2-N.

[51] M.F. Queiroz, K.R.T. Melo, D.A. Sabry, G.L. Sassaki, H.A.O. Rocha, Does the use of chitosan contribute to oxalate kidney stone formation? Mar. Drugs 13 (2015) 141–158, https://doi.org/10.3390/md13010141.

[52] N. Vlachos, Y. Skopelitis, M. Psaroudaki, V. Konstantinidou, A. Chatzilazarou, E. Tegou, Applications of fourier transform-infrared spectroscopy to edible oils,

Anal. Chim. Acta (2006) 459–465, https://doi.org/10.1016/j.aca.2006.05.034, 573–574.
[53] J. Xu, Z. Fan, L. Duan, G. Gao, A tough, stretchable, and extensively sticky hydrogel driven by milk protein, Polym. Chem. 9 (2018) 2617–2624, https://doi.org/10.1039/c8py00319j.
[54] S.M. Alshuiael, M.A. Al-Ghouti, Multivariate analysis for FTIR in understanding treatment of used cooking oil using activated carbon prepared from olive stone, PLoS One 15 (2020), https://doi.org/10.1371/journal.pone.0232997.
[55] A. Schönemann, H.G.M. Edwards, Raman and FTIR microspectroscopic study of the alteration of Chinese tung oil and related drying oils during ageing, Anal. Bioanal. Chem. 400 (2011) 1173–1180, https://doi.org/10.1007/s00216-011-4855-0.
[56] T. Wang, Y. Li, F. De Witte, F. Rebry, H. Li, P. Vermeir, K. Dewettinck, P. Van der Meeren, Influence of calcium concentration on the re-assembly of sodium caseinate into casein micelles and on their renneting behavior, Food Res. Int. 180 (2024) 113991, https://doi.org/10.1016/j.foodres.2024.113991.
[57] T. Zhu, J. Wu, N. Zhao, C. Cai, Z. Qian, F. Si, H. Luo, J. Guo, X. Lai, L. Shao, J. Xu, Superhydrophobic/superhydrophilic Janus fabrics reducing blood loss, Adv. Healthcare Mater. 7 (2018) 1086, https://doi.org/10.1002/adhm.201701086.
[58] D. Zhong, H. Zhang, Z. Ma, Q. Xin, Y. Lu, P. Shi, M. Qin, J. Li, C. Ding, Recent advancements in wound management: tailoring superwettable bio-interfaces, Front. Bioeng. Biotechnol. 10 (2022) 6267, https://doi.org/10.3389/fbioe.2022.1106267.
[59] M.D. Figueroa-Pizano, I. Vélaz, F.J. Peñas, P. Zavala-Rivera, A.J. Rosas-Durazo, A. D. Maldonado-Arce, M.E. Martínez-Barbosa, Effect of freeze-thawing conditions for preparation of chitosan-poly (vinyl alcohol) hydrogels and drug release studies, Carbohydr. Polym. 195 (2018) 476–485, https://doi.org/10.1016/j.carbpol.2018.05.004.
[60] C.N. Cheaburu-Yilmaz, O. Yilmaz, F. Aydin Kose, N. Bibire, Chitosan-Graft-Poly(N-Isopropylacrylamide)/PVA cryogels as carriers for mucosal delivery of voriconazole, Polymers 11 (2019) 1432, https://doi.org/10.3390/polym11091432.
[61] M.J.D. Nugent, C.L. Higginbotham, Preparation of a novel freeze thawed poly (vinyl alcohol) composite hydrogel for drug delivery applications, Eur. J. Pharm. Biopharm. 67 (2007) 377–386, https://doi.org/10.1016/j.ejpb.2007.02.014.
[62] B.S. Chee, G. Goetten de Lima, D.M. Devine, M.J.D. Nugent, Investigation of the effects of orientation on freeze/thawed polyvinyl alcohol hydrogel properties, Mater. Today Commun. 17 (2018) 82–93, https://doi.org/10.1016/j.mtcomm.2018.08.005.
[63] M. Demeter, A. Scărişoreanu, I. Călina, State of the art of hydrogel wound dressings developed by ionizing radiation, Gels 9 (2023) 55, https://doi.org/10.3390/gels9010055.
[64] L.-O. Lamke, G.E. Nilsson, H.L. Reithner, The evaporative water loss from burns and the water-vapour permeability of grafts and artificial membranes used in the treatment of burns, Burns 3 (1977) 159–165, https://doi.org/10.1016/0305-4179(77)90004-3.
[65] M. Demeter, A. Scărişoreanu, I. Călina, State of the art of hydrogel wound dressings developed by ionizing radiation, Gels 9 (2023) 55, https://doi.org/10.3390/gels9010055.
[66] P. Wu, A.C. Fisher, P.P. Foo, D. Queen, J.D.S. Gaylor, In vitro assessment of water vapour transmission of synthetic wound dressings, Biomaterials 16 (1995) 171–175, https://doi.org/10.1016/0142-9612(95)92114-L.
[67] D. Queen, J.D.S. Gaylor, J.H. Ebans, J.M. Courtney, W.H. Reid, Preclinical evaluation of the water vapour transmission rate through burn wound dressings, Biomaterials 8 (1987) 367–371, https://doi.org/10.1016/0142-9612(87)90007-X.
[68] X.R. Li, J.J. Jia, Y.H. Yan, T.J. Ni, Comparative studies on interactions of l-ascorbic acid, α-tocopherol, procyanidin B3, β-carotene, and astaxanthin with lysozyme using fluorescence spectroscopy and molecular modeling methods, J. Food Biochem. 41 (2017) 12338, https://doi.org/10.1111/jfbc.12338.
[69] R.S. Holzman, D.E. Gardner, D.L. Coffin, Vivo inactivation of lysozyme by ozone, J. Bacteriol. 96 (1968) 1562–1566, https://doi.org/10.1128/jb.96.5.1562-1566.1968.
[70] W. Ekasurya, J. Sebastian, D. Puspitasari, P.P.P. Asri, L.A.T.W. Asri, Synthesis and degradation properties of Sericin/PVA hydrogels, Gels 9 (2023) 76, https://doi.org/10.3390/gels9020076.
[71] M. Minsart, S. Van Vlierberghe, P. Dubruel, A. Mignon, Commercial wound dressings for the treatment of exuding wounds: an in-depth physico-chemical comparative study, Burns Trauma 10 (2022) tkac024, https://doi.org/10.1093/burnst/tkac024.
[72] J.L. Drury, R.G. Dennis, D.J. Mooney, The tensile properties of alginate hydrogels, Biomaterials 25 (2004) 3187–3199, https://doi.org/10.1016/j.biomaterials.2003.10.002.
[73] L. Peng, Y. Zhou, W. Lu, W. Zhu, Y. Li, K. Chen, G. Zhang, J. Xu, Z. Deng, D. Wang, Characterization of a novel polyvinyl alcohol/chitosan porous hydrogel combined with bone marrow mesenchymal stem cells and its application in articular cartilage repair, BMC Muscoskelet. Disord. 20 (2019) 257, https://doi.org/10.1186/s12891-019-2644-7.
[74] S. Carrasco, L. González, M. Tapia, B.F. Urbano, C. Aguayo, K. Fernández, Enhancing alginate hydrogels as possible wound-healing patches: the synergistic impact of reduced graphene oxide and tannins on mechanical and adhesive properties, Polymers 16 (2024) 1081, https://doi.org/10.3390/polym16081081.
[75] G. Lan, S. Zhu, D. Chen, H. Zhang, L. Zou, Y. Zeng, Highly adhesive antibacterial bioactive composite hydrogels with controllable flexibility and swelling as wound dressing for full-thickness skin healing, Front. Bioeng. Biotechnol. 9 (2021) 785302, https://doi.org/10.3389/fbioe.2021.785302.
[76] Malvern Instruments Worldwide, A Basic Introduction to Rheology, 2023.
[77] F. Soto-Bustamante, G. Bassu, E. Fratini, M. Laurati, Effect of composition and freeze-thaw on the network structure, porosity and mechanical properties of polyvinyl-Alcohol/Chitosan hydrogels, Gels 9 (2023) 396, https://doi.org/10.3390/gels9050396.
[78] P. Rainho, M. Salema-Oom, C.A. Pinto, J.A. Saraiva, B. Saramago, D.C. Silva, A. P. Serro, Polyvinyl alcohol/casein hydrogels with oxymatrine eluting ability for cancer-related wound management, Biomater. Sci. 13 (2025) 2755–2766, https://doi.org/10.1039/D5BM00191A.
[79] T. Ahmad Khan, K. Khiang Peh, H. Seng Ch, Mechanical, Bioadhesive strength and biological evaluations of Chitosan films for wound dressing, J. Pharm. Pharmaceut. Sci. 3 (2000) 303–311.
[80] H. Matsumura, R. Imai, N. Ahmatjan, Y. Ida, M. Gondo, D. Shibata, K. Wanatabe, Removal of adhesive wound dressing and its effects on the stratum corneum of the skin: comparison of eight different adhesive wound dressings, Int. Wound J. 11 (2014) 50–54, https://doi.org/10.1111/j.1742-481X.2012.01061.x.
[81] A. Punjataewakupt, P. Aramwit, Wound dressing adherence: a review, J. Wound Care 31 (2022) 406–423, https://doi.org/10.12968/jowc.2022.31.5.406.
[82] M.M. Flores-Nieves, R. Castellanos-Espinoza, M. Estevez, L.A. Baldenegro-Pérez, J. F.G. Trejo, M.E. García, B.M. Cano, G.M. Soto-Zarazúa, B.L. España-Sánchez, Electrospun Casein fibers obtained from revalued milk with mechanical and antibacterial properties, Arab. J. Chem. 15 (2022) 104201, https://doi.org/10.1016/j.arabjc.2022.104201.
[83] M.A. Aziz, J.D. Cabral, H.J.L. Brooks, S.C. Moratti, L.R. Hanton, Antimicrobial properties of a chitosan dextran-based hydrogel for surgical use, Antimicrob. Agents Chemother. 56 (2012) 280–287, https://doi.org/10.1128/AAC.05463-11.
[84] T.J. Silhavy, D. Kahne, S. Walker, The bacterial cell envelope, Cold Spring Harbor Perspect. Biol. 2 (2010) a000414, https://doi.org/10.1101/cshperspect.a000414.
[85] Z. Breijyeh, B. Jubeh, R. Karaman, Resistance of gram-negative bacteria to current antibacterial agents and approaches to resolve it, Molecules 25 (2020) 1340, https://doi.org/10.3390/molecules25061340.
[86] M. Song, Q. Zeng, Y. Xiang, L. Gao, J. Huang, J. Huang, K. Wu, J. Lu, The antibacterial effect of topical ozone on the treatment of MRSA skin infection, Mol. Med. Rep. 17 (2018) 2449–2455, https://doi.org/10.3892/mmr.2017.8148.